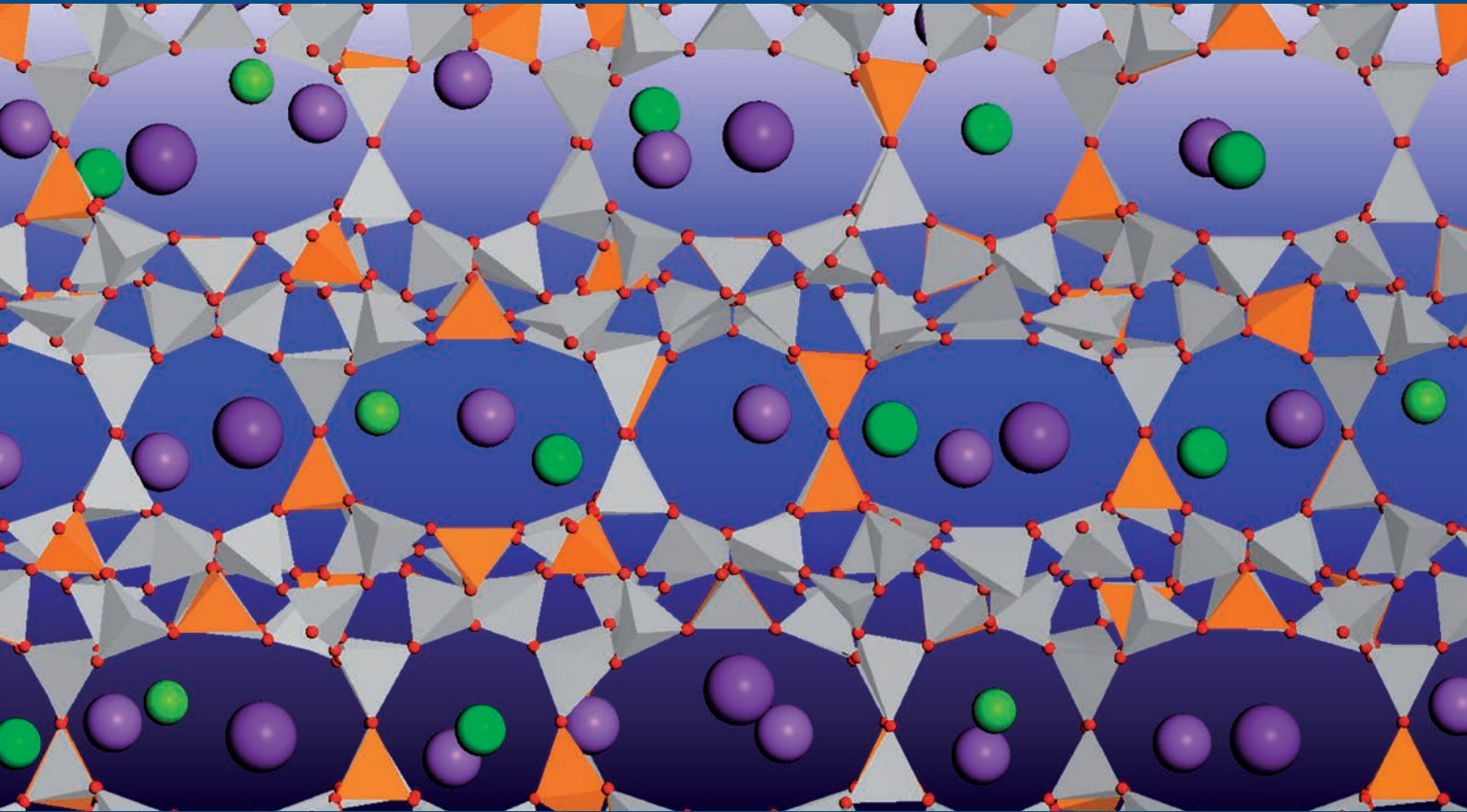


NNL Science

Issue 3 | 2015



Feature Article

USING CHEMICAL AND PROCESS MODELLING TO DESIGN, UNDERSTAND AND IMPROVE AN EFFLUENT TREATMENT PLANT

Also in this issue:

- Neptunium extraction in an advanced PUREX process and the EURO-GANEX process
- Density Functional Theory Calculations of the Actinide (VI) / Actinide (V) Redox Potentials in Water
- Muon Tomography: Characterising Legacy Nuclear Waste using Cosmic Rays
- Hydrogen yields from water on the surface of PuO_2

Contents

USING CHEMICAL AND PROCESS MODELLING TO DESIGN,
UNDERSTAND AND IMPROVE AN EFFLUENT TREATMENT PLANT 4 - 13

Scott Owens, Manon Higgins-Bos, Mark Bankhead and Jonathan Austin

NEPTUNIUM EXTRACTION IN AN ADVANCED PUREX PROCESS
AND THE EURO-GANEX PROCESS 14 - 20

Mike Carrott, Colin Gregson and Robin Taylor

DENSITY FUNCTIONAL THEORY CALCULATIONS
OF THE ACTINIDE (VI) / ACTINIDE (V) REDOX POTENTIALS IN WATER 21 - 24

Helen M. Steele, Dominique Guillaumont and Philippe Moisy

MUON TOMOGRAPHY:
CHARACTERISING LEGACY NUCLEAR WASTE USING COSMIC RAYS 25 - 29

Craig Shearer and David Mahon

HYDROGEN YIELDS FROM WATER ON THE SURFACE OF PuO_2 30 - 33

Howard Sims

NNL NEWS 34 - 35

- BEST Award
- Technical Conference
- DISTINCTIVE
- PHAROS

AUTHORS' BIOGRAPHIES 36 - 37

NNL PUBLICATIONS 38 - 39

Front cover: A representation of the atomic structure of Clinoptilolite from the Mud Hills area of California.

All material in this journal, including without limitation text, logos, icons, photographs and all other artwork, is copyright material of National Nuclear Laboratory Limited, unless otherwise stated. Material provided by any third party is likely to be the copyright of the author. Permission to copy or otherwise use such material must be obtained from the author.



Welcome to the third issue of “NNL Science”.

We have had very encouraging feedback on the two previous issues of NNL Science and I’m sure that there will be plenty to interest you in this edition.

With each issue, I myself always find fascinating examples of the excellent technical work which NNL have been doing, either for customers or funded by our own internal R&D programmes. This issue has a focus on our modelling work - sometimes a “Cinderella” area, which can be overlooked in favour of the more eye-catching projects we work on. Yet our modelling capability across the business is first-class, and the input from those teams underpins so many other aspects of what we do.

This will be my final issue of NNL Science, as I retire from NNL in Spring 2015. I’m delighted to be handing over the baton to the very capable hands of Professor Andrew Sherry who joined NNL in January 2015, and who will take over as Chief Scientist following my departure.

Graham Fairhall (Chief Science and Technology Officer)



Editor’s comments

Welcome to Issue 3 of the NNL Science journal. This issue contains a strong collaborative theme and highlights the value in scientific partnership between organisations with complimentary facilities and capabilities. A particularly good example is illustrated in our feature article where the computer modelling expertise within NNL is combined to build a predictive capability for an industrial plant: the Sellafield Ion Exchange Plant (SIXEP). Experimental data generated within NNL, supported by research performed at Universities, has helped to construct and validate models that enable our customers to make informed decisions about plant lifetime, feedstock requirements and contingency planning.

As our laboratory grows we understand that connections with other nuclear institutes across Europe will be essential because of the complexity of nuclear science and the expense in operating nuclear facilities. NNL has a strong relationship with the international actinide science community and this is well reflected in the award of a Eurotalents post with our French counterparts at CEA that has led to a body of work calculating the electrochemical potentials of actinyl (V/VI) species. NNL are taking a lead in the development of reprocessing flowsheets that provide control in the routing of neptunium, which has long been a problem element. Neptunium is long lived and can be mobile in the environment, so recycling it into new fuel provides some benefits. The radiochemistry team have developed methods where neptunium can be routed with the plutonium product for burning in new fuel in both advanced PUREX flowsheets and in a novel Euro-Ganex flowsheet, where the minor actinides (e.g. americium) are also separated. The latter flowsheet was demonstrated on irradiated fuel in hot cells in collaboration with the Institute for Transuranic Research (ITU), Germany.

Our close collaboration with the University of Glasgow has provided real benefit in the development of a novel analysis technique using muon tomography that allows the identification of high atomic mass materials in difficult to access areas. This kind of information supports robust decision making in, for example, the decommissioning of highly active cells to be made in, for example, decommissioning of highly active cells.

Finally I would like to congratulate our BEST award winner Howard Sims for his work on the radiolysis of water on PuO₂ surfaces that is helping to underpin the interim storage of plutonium at the Sellafield site. This work is contributing to an international effort to understand the behaviour of PuO₂ during years of sealed storage.

Mark Sarsfield (*Editor, NNL Research Fellow*)

mark.sarsfield@nnl.co.uk

Katie Bell (*Assistant Editor*)

katie.j.bell@nnl.co.uk

USING CHEMICAL AND PROCESS MODELLING TO DESIGN, UNDERSTAND AND IMPROVE AN EFFLUENT TREATMENT PLANT.

Scott Owens, Manon Higgins-Bos, Mark Bankhead and Jonathan Austin

scott.owens@nnl.co.uk

Introduction

The Sellafield site is currently undertaking programmed activities to make a significant advance in the retrieval and decommissioning its Legacy Ponds and Silos in order to remove hazards and wastes for long-term storage. The programme is scheduled for at least another 100 years, with an estimated cost in the tens of billions of pounds. This wide ranging cost estimate reflects the uncertainties and contingencies within the programme due to the considerable technical, environmental and operational challenges.

Wastes have been stored at the Sellafield Site for decades. These wastes have been generated over an extended timescale (1950s – present). In the case of legacy wastes (generated up to the early 1980's) there is some uncertainty about the condition of these wastes and the facilities they are stored in. This was due to poor record keeping at the time, and continued limited access due to high radiation hazards which poses challenges for sampling and detailed characterisation. Correspondingly there is an uncertainty of the future effluent arising that will be generated as part of the retrieval and decommissioning operations in terms of the volume generated and the chemical compositions. On Sellafield site, the Site Ion eXchange Plant (SIXEP) remains a key facility to support current operations.

Plants and processes that are intended to treat wastes and the associated effluent were designed to operate within specific feed envelopes in accordance with the Best Available Technology (BAT) principles. Not only is there a major drive for hazard reduction, there are also important environmental, health and safety drives to protect the workforce and minimise radioactive discharges into the environment.

The use of modelling tools is relied upon to understand and optimise the retrieval and decommissioning programmes. This is because modelling provides:

- A way to interrogate what process variables need to be known. This will inform future monitoring requirements and to define and underpin the feed and operating envelope
- An underpinning of technical risks because models help to illustrate the consequences of operating outside of existing feed and / or operating envelopes
- An up to date description of the technical processes that will in the future facilitate knowledge management

A suite of models are continuing to be developed and updated by both Sellafield Ltd and NNL. The models developed by NNL provide a detailed mechanistic description covering dynamic process engineering and chemistry models of speciation and chemical reactions. The NNL suite of models are under continued development to be used in the support of the retrieval and decommissioning programmes. Such models will

ensure that confidence can be given to the projected retrieval schedules which safeguard the retrieval and subsequent decommissioning programme. This will enable Sellafield to meet their regulatory requirements and their cost and time estimates.

The paper describes the method developed by NNL for developing mechanistic models in accordance with the BAT principles. To do this it starts with the development of a model of the Sellafield Site Ion eXchange Effluent treatment Plant (SIXEP) and how a range of modelling tools – from atomic scale to plant dynamic flowsheets – have come together to predict the future performance of the plant. It then goes on to describe how experimental work and modelling have been used to underpin such models. The reader will learn why modelling has been invaluable to operators in understanding and improving their effluent treatment plants.

The Sellafield Site Ion Exchange Effluent Treatment Plant (SIXEP)

Key to the Sellafield Site minimising its impact on the environment is SIXEP. The plant was designed to remove the major contributors to soluble activity (predominantly Cs-137 and Sr-90) and alpha emitting particulate material from pond effluents before sea discharge. Consequently, SIXEP has had a huge impact in reducing radioactivity in sea discharges since its opening in 1985 (Fig. 1).

At the time of design and during early operation, the effluent sent to SIXEP for treatment were considered homogeneous in composition, which is an important requisite for a well designed ion exchange treatment process. With time, the effluents sent to SIXEP, became more heterogeneous in nature and the requirement to demonstrate understanding of the process and continued good management facilitated the development of the SIXEP model.

Continued good management of SIXEP has ensured the plant's successful (and improving) operation. With an imminent gear change in retrieval operations, and the imminent closure of several operating plants on the site the demands being placed on SIXEP and related effluent treatment plants are going to increase. Therefore, the need to understand and quantify the risks associated with these changes in operation, to continue to meet environmental obligations, is even more relevant now and into the future.

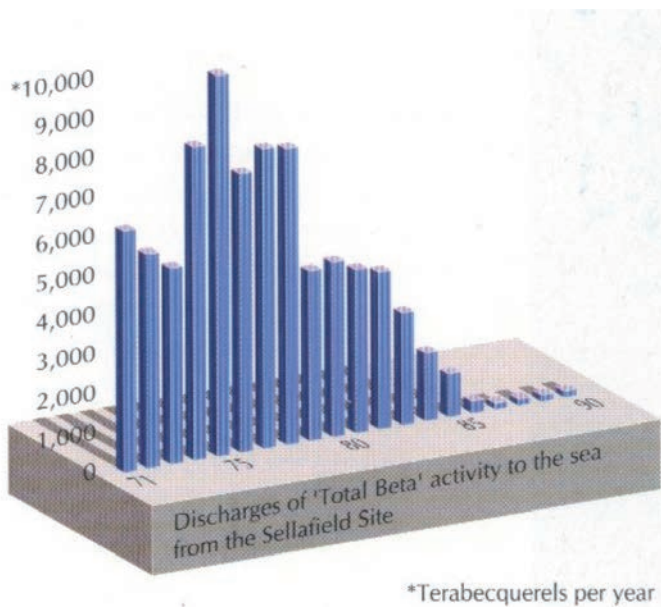


Figure 1: Chart of Sellafield Sea Discharges – Beta Activity

The SIXEP Process

The name SIXEP implies the use of a single process operation, however it is actually a sequence of effluent treatment processes, designed to condition wastewater from a wide range of plants and make them suitable for discharge to sea. A simple summary of the process is shown in Fig. 2.

It consists of the following units:

- Settling tanks that allow large particulates to settle from feed solutions before they are fed to the sand beds. Further details are provided in section "Solids Removal (Settling)".
- Two sand bed filters operate in parallel to remove small quantities of suspended solids to protect the ion exchange beds from blinding and to reduce the soluble Mg^{2+} concentration. A quaternary amine polyelectrolyte flocculant is added to the solution prior to the sand bed to improve filtration performance. See section "Solids Removal (Filtration)".
- A carbonation tower, which adjusts the pH of the solution emerging from the sand bed from ~ 11.2 to \sim pH 7 in order to protect the clinoptilolite beds, which degrade at high pH. See section "Liquor Neutralisation".
- Two clinoptilolite beds, which operate in series (one lead bed and one lag bed). The lead bed is replaced with fresh media when it is exhausted, and the bed that previously operated in the lag position is promoted to the lead position. See section "Modelling Ion Exchange".

Modelling and Experiment

Although this article is devoted to the SIXEP Chemical Model and the modelling work that has been used to provide additional mechanistic understanding, it is very important to recognise that throughout the development of the model there has been a very close link between the modelling work, plant validation and experimental (laboratory and small scale rig) programmes.

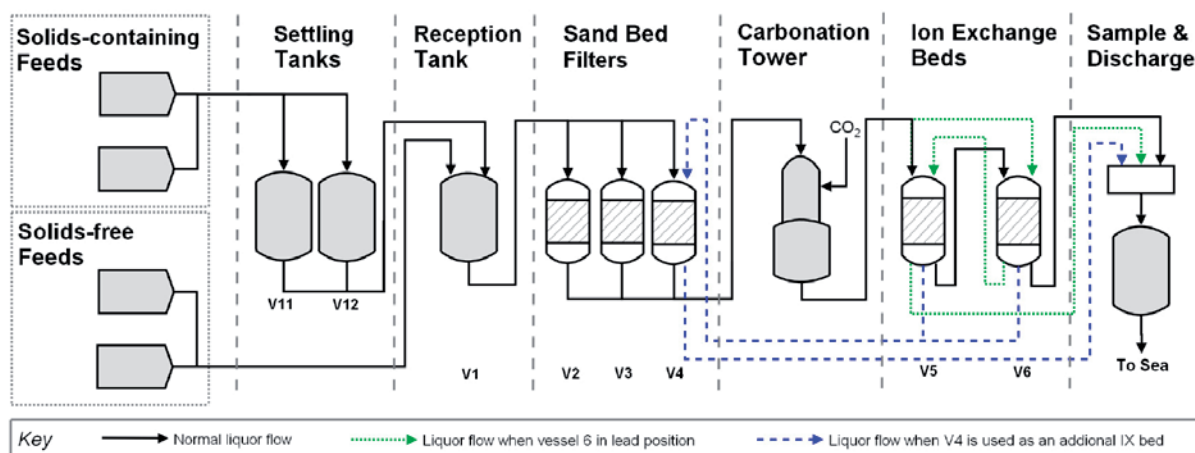


Figure 2: Process diagram of SIXEP

The success of the current model is due to the process of refinement of understanding. Confidence in the model mechanisms is improved by testing against plant data, experimental work raises the “questions” that the model needs to address and provides the data to parameterise and validate the models.

A good example of this approach – integrating modelling and experiment – (for another ion exchanger not used in SIXEP) is shown in [1, 2] undertaken with the University of Salford. In recent years, this has expanded to include understanding gained from modelling other plant and processes on the Sellafield site and throughout the UK nuclear estate.

The SIXEP Chemical Model

The SIXEP Chemical Model evolved initially from a simple dynamic process model of the ion exchange columns, designed to replicate how small changes to feed activity would impact on effluent leaving the plant. Throughout the model’s evolution and development, the focus has always been on trying to understand plant behaviour, not simply to replicate it.

Quoting from the FGMSP effluent strategy (endorsed by the regulators)

“The dynamic SAMP flowsheet offers the capability for performing dynamic activity and mass balances across the effluent stream, including MSSS batch feeds via EDT centre chamber. The SIXEP ion exchange model is a mature tool developed by NNL and applied successfully to new feeds over several years. In combination the two models offer the means of predicting SIXEP performance when challenged with new feeds. SIXEP expects FGMSP and MSSS to apply these tools in support of environmental impact assessments.”

The following discussion will proceed from plant feed through to sea discharge, however it is important to realise that the chronological order of development has been more usually in the reverse direction – reflecting the constant focus on getting the predicted plant effluent correct. The work is far from exhaustively represented here with representative examples being given of the modelling approaches used.

The SIXEP Chemical Model has been implemented in the gPROMS. The gPROMS software allows a model of a plant or a process to be built from a collection of component models, linked together through connection streams [3]. The behaviour of the individual components can be defined using sets of time dependent differential and algebraic equations that have been designed to represent the chemical and physical processes that occur therewith. This approach allows a “plant” to be built within a model in very much the same way as a real plant would be built, from a set of component parts, linked together.

Plant Feed

SIXEP is designed to condition and remove activity from aqueous effluent arising in Magnox storage and treatment infrastructure on the Sellafield site – particularly Magnox ponds and silos. Most of the high volume feed to SIXEP is alkaline, to reduce Magnox corrosion ($\text{pH} > 11$) and contains a range of soluble radioisotopes – particularly caesium and strontium. These are the two highest concentration, most mobile radioactive species, arising in aqueous environments in contact with spent nuclear fuel – resulting in them being the biggest contributors to activity and dose in aqueous effluent streams arising in most nuclear facilities. The feeds often contain entrained solid material (particularly “sludge” from fuel and cladding corrosion – a mixture of uranium metal, Magnox alloy, brucite, uraninite and hydrotalcite), a number of other soluble active isotopes, and significantly larger concentrations of non-active dissolved cations (primarily sodium, magnesium, calcium, potassium).

The plant routinely operates on the basis of feeds meeting “Conditions for Acceptance” (CfA). The SIXEP Chemical Model has been used to underpin the range of feed compositions that comprise the CfA, to give a high confidence that SIXEP can reliably treat streams that meet these conditions. However, in the future, predicted future feeds to SIXEP may not meet the CfA for periods of time, so the SIXEP Chemical Model has been used to predict the impact of these streams, and determine whether they are going to be acceptable to SIXEP. Examples of some of these studies are given later.

The main feeds to SIXEP in terms of volume are from Magnox fuel storage ponds, at approximately 700,000 m³ per year. A range of modelling tools have been used to augment sample analysis to provide a more full understanding of the chemistry of the SIXEP plant feeds, necessary to give good predictions of plant performance. Some examples of these are listed overleaf (Fig. 3).

A process engineering model (also implemented in gPROMS) is used to predict the volume and composition of effluent leaving the main operating feed source pond for SIXEP from a knowledge of long term fuel chemistry behaviour in the pond, scheduled pond operations (such as arrival of new fuel, movement of fuel skips and reprocessing of fuel) and the waste arising from them (such as liquor activity and the mass of corroded Magnox sludge leaving via a range of routes – including to SIXEP). This model takes its future schedule from timetabled plant requirements and produces output such as that shown in Fig. 3. This model is regularly validated by comparing plant predictions against current and past performance as shown.

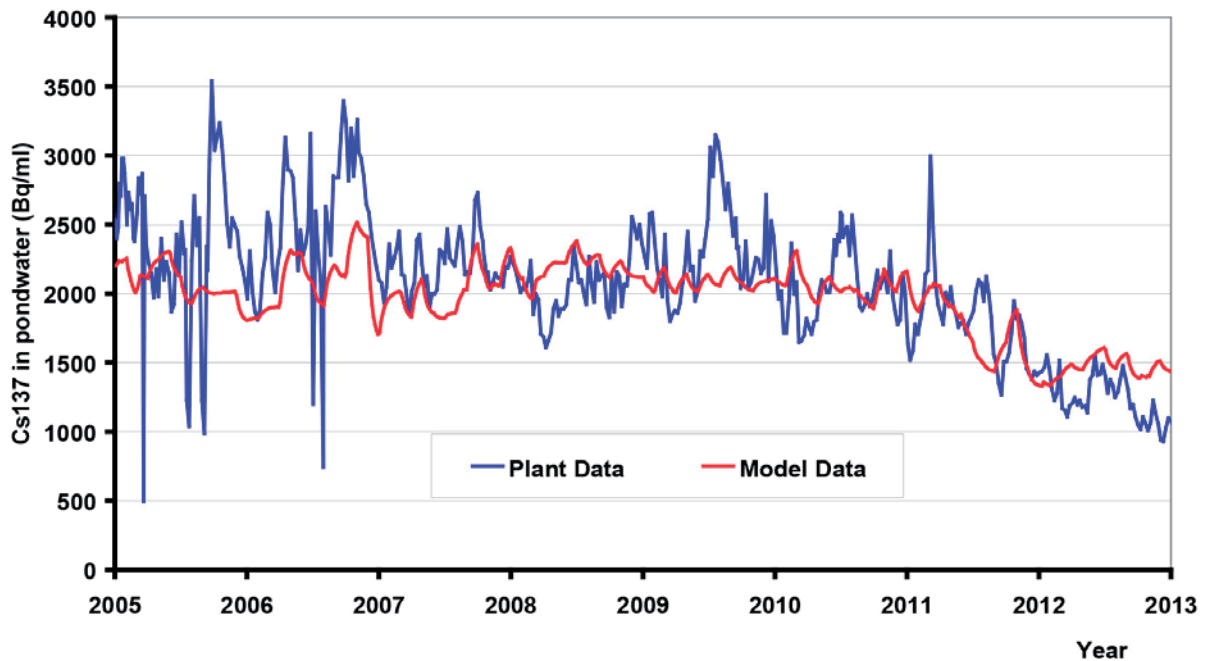


Figure 3: Cs-137 activity predictions within the Fuel Handling PLant (FHP) pondwater

More general understanding of the solubility of species is given through thermodynamic modelling techniques. This approach predicts the most stable thermodynamic products of a chemical reaction sequence; for example stable solid phases, soluble speciation and limits of solubility. It can be enhanced to include chemical kinetic models that predict not only what the thermodynamically-stable phases are, but how fast they arise from the initial composition specified. The main codes used in NNL for thermodynamic modelling are PHREEQC [4] for aqueous chemistry (including environmental models) and MTDATA [5] for all other chemistry and materials applications (such as fuel modelling).

A series of PHREEQC speciation assessments have provided supporting understanding, why the SIXEP ion exchange process does not provide effective abatement performance for certain radioisotopes such as antimony, technetium and certain plutonium species, as these were shown to be present in an anionic form (e.g. antimonite, antimonite and pertechnetate). The SIXEP ion exchange process is based on cation exchange, hence the anionic species are outside of SIXEP design intent.

Two further PHREEQC speciation studies are described in later sections (see sections "Solids Removal (Settling)" and "Modelling Ion Exchange").

Solids Removal (Settling)

Much of the recent model development work associated with SIXEP and effluent treatment generally, has been in the identification and removal of solids entrained in the various feed streams. These include a wide range of particulate debris, corrosion products, precipitated solids and colloidal material, and they

can carry a significant amount of activity; at the very minimum they will block the ion exchange beds and associated filters at the end of the plant.

There are two solid removal processes associated with SIXEP:

- settling tanks, which remove larger solid particulates from a smaller range of streams known to have a high solid loading
- sand bed filters, which remove finer particulate material, including some colloids.

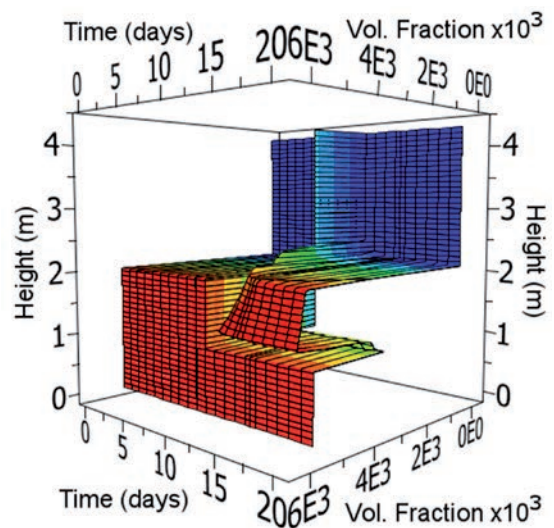


Figure 4: Modelled disturbance of a sludge bed

In the settling tanks (as the name implies- though they are also commonly called "Bulk Storage Tanks") high solid-loaded feeds are received and left to settle (there are two tanks and they are used in rotation). In addition to their intended purpose of removing and storing particulate solids, these tanks have been found to behave as a "buffer store" for certain species,

particularly strontium – storing activity in times of high challenge to the plant and releasing it slowly during periods of lower challenge. This was observed in plant analysis of Sr-90 during periods of feed pond routine shutdown. Experimental investigation of the interaction of simulated sludge solids with strontium showed this uptake, but interestingly and somewhat surprisingly, also showed the phase most responsible for this behaviour wasn't brucite ($MgOH_2$ – formed from corrosion of Magnox metal and by far the most common phase in sludge) but minor uranium corrosion phases such as uraninite.

This part of the SIXEP Chemical Model comprises two processes – solid settling and exchange of species between the solid and liquor phases. It was developed using a range of settling experiments, adsorption and solubility experimental studies (for example the adsorption of strontium by uranium and Magnox phases and solubility of brucite), thermodynamic modelling and fitting to reduced-scale plant simulation studies (Fig. 4, 5 and 6). These combine to give a well-supported mechanistic model of how solids settle in this process, and how this affects the concentration of species in the liquor passing through the tank. As a result, the effect that this part of the plant has on the later stages is now predictable.

Fig. 6 shows one interesting example of output obtained

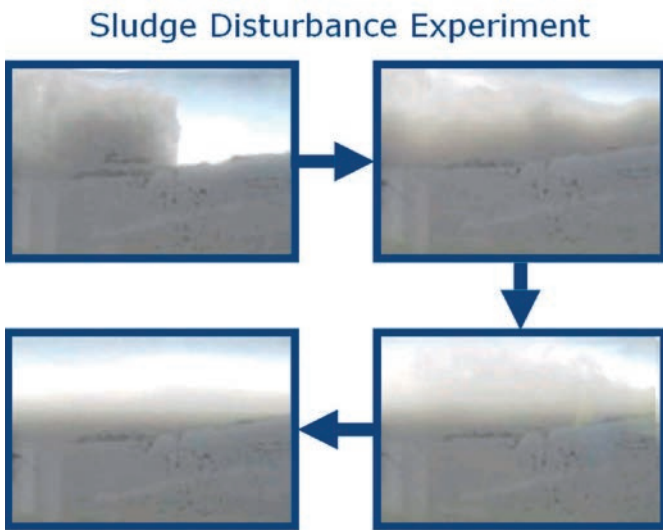


Figure 5: Settling studies of Magnox sludge corrosion products

from the settling model. The three dimensional plot shows the evolution of a bed of mixed sludge material following re-suspension of the solids. Here, time is increasing from left to right (up to 206 hours) depth within the bed from bottom to top (of 4m) and particle concentration from back to front. The results show clearly a stratification of the sludge on settling – with the denser uranic material concentrating in layers at the bottom of the settling tank.

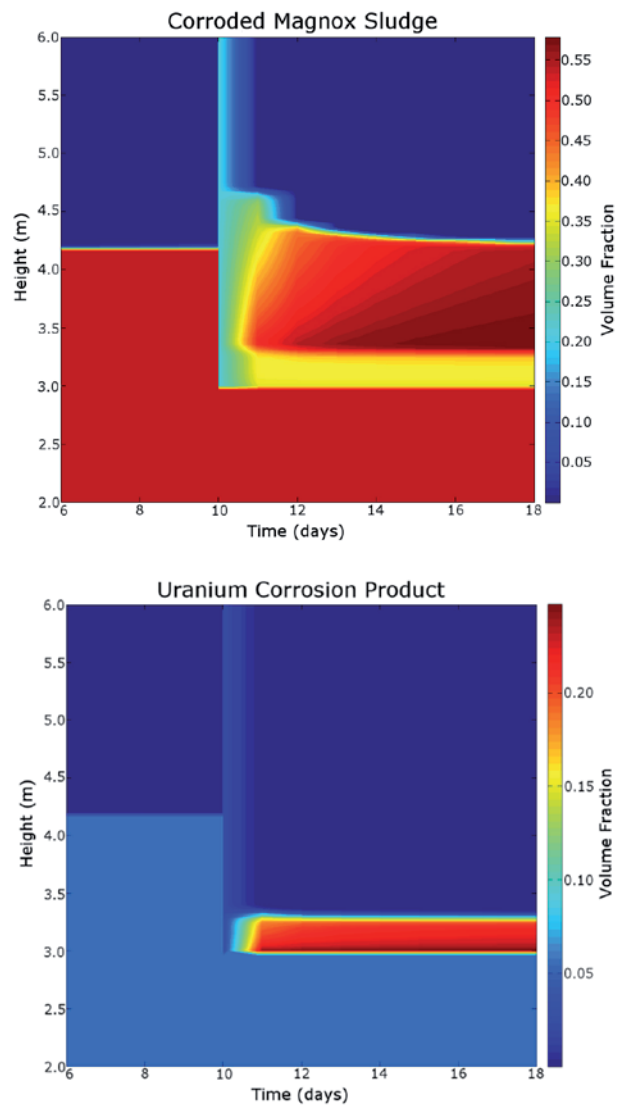


Figure 6: Settling Studies of Magnox Corrosions Products. Upon disturbance, Corroded Magnox Sludge may become separated from Uranium Corrosion Products.

The buffering of radionuclides by these settling tanks is important for the prediction of the activity challenge to the ion exchange stage of SIXEP. This buffering is modelled by two mechanisms in the settling tank models. Firstly, release through dissolution of magnesium-based solids following a drop in pH. Fig. 7 shows the change in solubility of magnesium with pH.

Secondly the model captures the surface adsorption-desorption behaviour of radionuclides on the solid phases, which is also pH dependent. Adsorption and desorption is modelled using distribution coefficients (K_d) which have been parameterised against experimental studies at various pHs.

$$K_d = \frac{\text{activity per g}}{\text{activity per ml}} = \frac{A_{tot} - A_{aq}}{A_{aq}} * \frac{V}{M}$$

where A_{tot} is the total activity in the system (Bq), A_{aq} is activity associated with the liquor in the system (Bq), M

is the mass of the solids (g) and V is the volume of the system (mL), giving units for K_d of mL/g.

This work has had a significant impact on other parts of the Sellafield site, in that the same approach has been used to help improve design of other plants needed to remove similar solids from decommissioning operations. Also, this has led to a requirement to understand the behaviour of solid containing liquors of high pH over long stagnant periods, where atmospheric carbon dioxide will reduce the pH of the liquor, and possibly lead to a change in the solubility of those solids (Fig. 7).

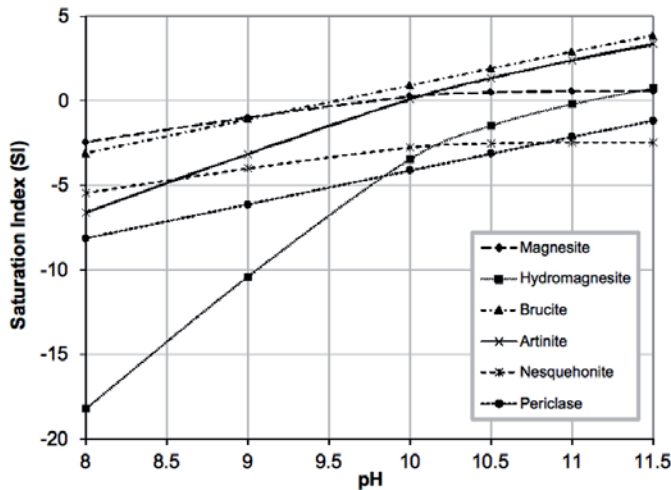


Figure 7: Solubility of magnesium-containing solids as a function of pH (PHREEQC)

Solids Removal (Filtration)

The filtration stage of SIXEP removes any remaining fine particulate material using two parallel vessels containing sand coated with a polyelectrolyte to enhance sticking. Built up particulate material is removed, and the beds recharged, by fluidising and back washing the bed.

This process again is highly effective; however, uncertainties due to feeds from decommissioning operations containing different solids, particularly fine colloidal material, have required that the process of particulate uptake be understood in more detail. This work is new and ongoing with previous experimental research undertaken at the University of Manchester (through a PhD, funded by Sellafield Ltd and undertaken as part of an NNL staff secondment) and is being integrated into a modelling framework [10].

Initial coarse grained molecular dynamics (see later) for detailed description of molecular dynamics modelling work at the NNL sought to understand how entrained particles and colloidal material sticks to the sand – with particular emphasis on the role that polyelectrolyte (a soluble polymer added to the feed that improves performance of the sand filter) plays in filtration of colloidal material. Below (Fig. 8) are

snapshots of simulated interactions – showing clearly how the polyelectrolyte aggregates to the surface of the sand, and how the colloidal particles congregate near the polyelectrolyte.

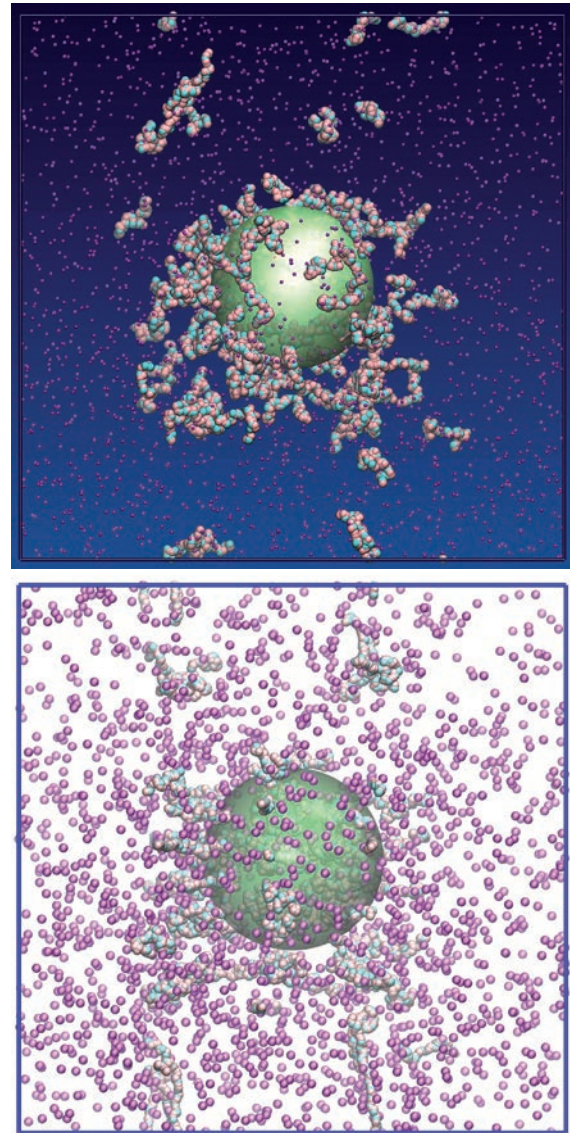


Figure 8: Sticking of polyelectrolyte (top) and colloids (bottom) to sand particulates

Work in the immediate future with the University of Liverpool, is looking to build a detailed mechanistic model of the sand bed incorporating understanding from work like this. Understanding this stage is essential for the future success of the SIXEP plant, as over 90% of the actinide activity in the feeds is removed by the sand beds and continued improvements in understanding are required to predict the impact of some significant changes to the feed arising from future decommissioning operations.

Liquor Neutralisation

The final adjustment to the liquor chemistry before it is passed to the ion exchange columns is undertaken in the plant carbonation stage. This comprises a “tower”

filled with packing rings and a “sump” which stores the liquor ready for pumping to the ion exchange columns. The effluent liquor is pumped in at the top of the tower and trickles down through the packing rings, where it is contacted with carbon dioxide being pumped in the opposite direction. Alkaline solutions readily absorb CO₂ and the liquor is brought to neutral pH through the formation of hydrogencarbonates and carbonates. This process requires little “management”, because as the liquor approaches neutral pH, the solubility of carbon dioxide decreases dramatically – so the neutralisation slows and stops as pH 7 is reached.

However, there are other consequences of this process on the liquor. As seen several times in this article, changing the pH of the liquor also changes the solubility of many species. As a result, any magnesium based solid (or more commonly colloidal material) that breaks through the filtration stage is dissolved here. Good plant management ensures that this does not appear to be a problem for SIXEP, however the mechanistic understanding obtained from work on this mechanism has led to the ability to predict the rate that Magnox sludge will dissolve if left in contact with air. This in turn is important in predicting SIXEP feed compositions.

Modelling Ion Exchange

The two ion exchange columns are placed in series and are operated in what is called a “carousel” operation. The first column in series is referred to as the “lead” column and the second the “lag” column. The ion exchange columns are fed until there is a breakthrough of activity on the lag column. Then, through a change of flow through the plumbing of the columns, the lag bed is placed in lead position, the lead column is taken temporarily off-line while its spent ion exchange material is replaced with fresh ion exchanger. Following clean out, the fresh column is placed in the lag position and flow re-started through the column. This procedure maximises the amount of activity taken up by the ion exchanger, and therefore minimises the amount of spent ion exchange material produced.

It is this stage where the caesium and strontium (and some residual soluble actinide) activity is removed from the effluent liquor. Most process engineering models of ion exchange for effluent clean-up treat ion exchange columns as though they are adsorbing columns – considering only the activity sticking to the exchanger and ignoring the effects of desorption and ion competition. For many examples this is a reasonable simplification, particularly if the feed is fairly constant and the activity levels fairly low but in this instance desorption was required to fully predict plant performance.

The models consider each ion exchange column to be a cylinder, with fluid flowing uniformly from the top

to the bottom. This allows the model to consider the variation in concentration as being one-dimensional – i.e. concentration changes down the column, but is uniform at any specific depth.

The current model of the ion exchange column is made up of five components:

1. fluid flow down the column
2. dispersion (broadening) of the concentration profile
3. exchange of ions between the fluid phase and particle
4. transport of ions through the particle
5. exchange of ions within the particle.

These combine to give a profile of the concentration of species in the column liquor and the concentration of exchanged ions on the ion exchanger, with depth – and this is used to predict the concentration of the liquor leaving the bottom of the ion exchange columns. As the two columns are in series, the effluent from the “lead” column is fed into the “lag” column. The evolution in concentration profile due to fluid flow is modelled simplistically through a local flow rate and concentration gradient.

Dispersion describes the effects of inter-particle fluid “turbulence” – i.e. a spike of concentration at the top of the column becomes significantly broadened as it progresses through a column due to the mixing caused by fluid swirling around particles and squeezing between them. This is important in predicting the shape of the activity profile. It is modelled through an enhanced diffusion-like mechanism.

The final three processes describe ion exchange between the mobile fluid phase and the static ion exchange material phase. Early versions of the model considered the column to be homogeneous and well-mixed at any depth – i.e. there was no representation of the ion exchange particles, and therefore processes 3&4 were not modelled explicitly. As a result, the final three processes were considered in one kinetic mechanism. Interestingly, this turns out to be a much better representation than might be imagined – for reasons that will be explained later.

The final version of the model added another dimension to the ion exchanger concentration – modelling concentration with particle radius at any given depth in the column. This model includes a full description of transport between the bulk fluid and the particle surface, transport of species through the particle and ion exchange chemistry (mechanisms 3-5). This version of the model is computationally slower but considerably more versatile. This model finds its most common applications where the ion exchange column can no longer be considered “well-designed” – high or low fluid flow rates, fine ion exchange particles and high concentrations of active cations. Exchange of ions

between the fluid phase and the particles has been modelled assuming film diffusion – i.e. there is a stagnant layer around the particle that the ions must diffuse through. This is also being enhanced by current studies of fluid flow within particle beds (mentioned earlier), but is currently modelled using simple engineering correlations of film diffusion.

Ion exchange kinetics are assumed to follow the same rate laws throughout the columns, and are a strict mass-balanced exchange process. They have been from the start mediated entirely through sodium exchange, as sodium is in vast excess in both the ion exchanger and the feed solution in SIXEP. In the following sections, the approach to developing and parameterising this model will be described and the “mystery” of why a particle-based model does not seem to be always necessary, will be shown.

The ion exchange beds comprise an ion exchange material called clinoptilolite; a natural zeolite found extensively in the earth’s crust and obtained – for SIXEP – from a large deposit in the “Mud Hills” area of California. Since the 1960’s it has been known that clinoptilolite possessed the ability to selectively ion exchange caesium and strontium isotopes from aqueous solutions in the presence of other common cations [7].

Natural clinoptilolite has a wide-ranging composition, depending on where it has evolved (though always with the same crystal structure – Mud Hill natural clinoptilolite shown below in Fig. 9), and this specific deposit has shown the best uptake for caesium and strontium with a tolerably small variation in composition.

In zeolitic ion exchange materials there is a regular, crystalline porous framework based on silica, and everywhere that a silicon ion is replaced with an aluminium ion there is a resultant negative charge on the framework. As the material must be charge neutral, this negative charge is balanced by cations located in the framework channels and cages. These “extra-framework cations” are mobile, particularly when the zeolite is solvated, and they can be exchanged – within the zeolite and (at the external surface) with a contacting solution. Thus zeolites are cation exchangers. In Fig. 9, the framework is made up of orange SiO_2 tetrahedra and pink AlO_2 tetrahedra – arranged in layers supported by bridges – to give a two dimensional pore network. The pores that form the spaces between the layers are filled with a range of cations – K^+ (large, light blue), Na^+ (purple), Sr^{2+} (red) Ca^{2+} (larger, darker green) and Mg^{2+} (small lighter green). These cations are surrounded and solvated by (red and white) water molecules.

Different zeolites show a preference for different cations. Clinoptilolite is particularly selective for caesium and strontium ions. This is partly due to thermodynamic drivers and partly kinetic. A long history of atomic scale modelling research on this material and materials like

it has been undertaken by NNL, with examples of some of the studies of the mechanism given in [8, 9].

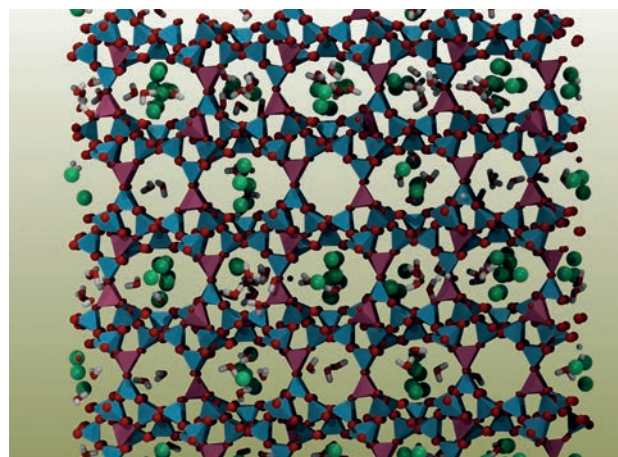


Figure 9: Crystal unit cell of Mud Hills natural clinoptilolite

The thermodynamic drivers are due to the size and shape of the channel structure, which favours large cations; and the relatively small concentration of aluminium in the framework (generating a low charge density gradient), which favours large monovalent cations. Thus caesium, being the largest monovalent cation, is strongly retained on thermodynamic grounds. Strontium selectivity is less easy to understand, as it is a smaller divalent cation. However examination of the strontium speciation in solution (using PHREEQC, see previous section “Plant Feed”), along with molecular models of these species, shows that a small, but significant proportion of the strontium is present in the feed liquor as hydrogencarbonate $\{\text{SrHCO}_3\}^+$ or hydroxide $\{\text{SrOH}\}^+$ complexes. This strontium fraction, with an effective size and charge density that mimics that of Cs^+ , has a significantly better selectivity in clinoptilolite than expected from the divalent species. This speciation is particularly important in the kinetic ion exchange process.

The kinetic process involves the combination of narrow pores of clinoptilolite and the diffusion rate of cations in aqueous solution. Because there is much less interaction between large ions of low charge with polar water molecules, big, monovalent cations like caesium diffuse much faster through aqueous solution than small, highly-charged cations like magnesium. This is emphasised inside the clinoptilolite channels, where the mix of framework charge and water polarity retards the movement of “charge dense” cations significantly. As a result, caesium, potassium, and to a lesser extent strontium, are preferentially exchanged into clinoptilolite by both mechanisms (i.e. kinetic and thermodynamic ion exchange).

Transport of ions within clinoptilolite has been modelled using the Fickian diffusion method. Unfortunately, the idea of “diffusion” of ions inside zeolites is an oversimplistic one. Confinement and constriction needs

to be included as these simply modify the geometric freedom of this statistical process occurring. However ion exchange is difficult to integrate, because movement of cations inside the zeolite has to be a cooperative process to preserve overall charge neutrality – therefore “diffusion” inside the zeolite is not an entirely random process.

So to develop and parameterise a model of transport of ions through a zeolite particle needs a different approach. Maintaining charge neutrality is comparatively easy – reversible, mass-balanced chemical reaction kinetics are used on a bulk scale model of the material (e.g. of the order of microns or larger). The “diffusion” coefficient has to be modelled at a molecular scale using molecular dynamics.

Molecular dynamics {molecular dynamics} is a technique where a geometric model of a molecule or material is constructed from the constituent atoms connected by representative bonding forces and is evolved in time under a set of constraints (for example temperature, pressure, total energy, volume). This simulates how the position of atoms and molecules (and the bonding forces between them) evolve with time. This fundamental technique can be used to make predictions about many properties of molecules and materials including vibrational spectra, thermal properties (such as heat capacity and thermal conductivity), structural properties (such as density and dimensional change) and mechanical properties (such as Young’s and elastic moduli and fracture stress). Transport properties such as diffusion are a base output of this approach (the overall movement of atoms or ions) and so diffusion coefficients are easily calculated. This simulation method is more like an experiment than anything truly “theoretical” as the model does not assume a mechanism for diffusion, but “measures” it through the progress of the simulation. Thus the “diffusion” coefficient (or whatever you might wish to call this transport coefficient within a zeolite) is representative of the material composition used.

When these diffusion coefficients were obtained, they were found to be extremely small – many orders of magnitudes smaller than in free solution. This seemed to agree with the general observations reported in the literature for experimental determinations in zeolites. When the values were input to a diffusion model of particle, using a typical concentration for caesium in the fluid feed to the columns, it was found that over the course of a typical residence time of zeolite in a SIXEP bed (144-180 days) caesium only penetrates a few microns into the particle. As the solution is effectively

only interacting with the outer layer of the exchanger particle under normal conditions, this explains why a particle-based model is not required to predict caesium (and strontium) abatement by the column. Hence, under normal plant operating conditions, the kinetic ion exchange rates of reaction, mediated by sodium exchange, suffice.

The particle diffusion model description does become important for example, when investigating the longer-term storage conditions of the loaded clinoptilolite and the potential for activity leaching.

Simulation of SIXEP Plant Performance

Over recent years, this model has been used to predict the performance of the SIXEP plant for a wide range of feeds, and has been validated against SIXEP performance.

Comparison between prediction and past performance are shown below in Figure 10.

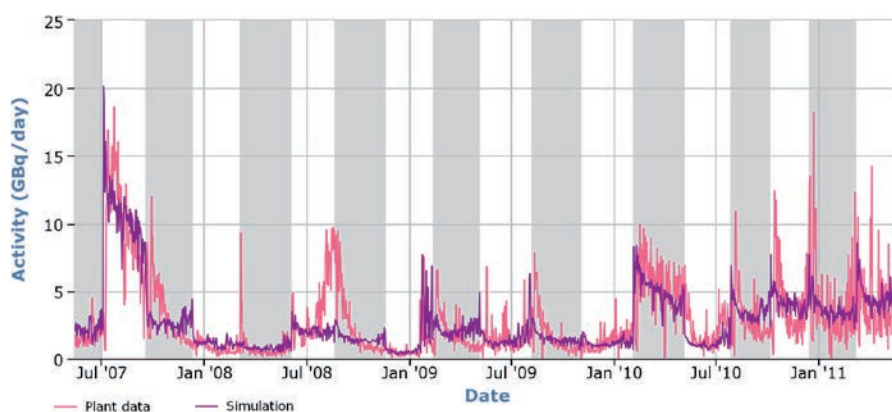


Figure 10: Comparison between recent SIXEP performance and model predictions for Cs-137 discharges (grey bands indicate bed changes)

It is important to recognise that Figure 10 shows the comparison between real plant data and a model that comprises mechanistic models of a sequence of complex processes - it is not simply a fit to observed plant performance. As a result, it can be (and is) used to underpin strategic decisions on plant operation, and to help justify these decisions to the UK regulators.

The model has also been used to help understand other aspects of the plant’s performance. A good example of this is the unusual “U” shaped profile, usually seen for caesium breakthrough in SIXEP. Column breakthrough should generally follow an “S” shaped profile (such as that seen for strontium) with concentration breakthrough being initially zero, and rising after a period of time until it levels out at the inlet concentration.

Caesium however usually shows a significant initial breakthrough concentration following an ion exchange bed change. A number of processes and mechanisms were suggested for this breakthrough and each were tested using the model. In the end, the only mechanism that showed the required initial

caesium breakthrough assumed that there is caesium-loaded ion exchange material at the bottom of the column immediately after the bed is changed. In other words, some ion exchange material remains after a bed change – and according to the simulations, this does not have to be a significant amount of material. This has contributed to improved bed changing procedure and the implementation of routine camera inspections.

Further uses of the model include:

- Predictive model for ion exchange with both natural and pre-treated forms of clinoptilolite; supported the pre-treatment plant trials and the technical justification for when to use pre-treated clinoptilolite on plant (sustained increased feed challenge / when current stock has run out).
- Underpinning the SIXEP CfA for competing ions and pH, where the SIXEP modelling showed the consequences of operating outside of the current CfA. The link between pH and strontium / magnesium solubility was underpinned by experiments and data assessments, but this has subsequently been incorporated into the NNL settling models (see previous section “Solids Removal (Settling)”).
- Used to underpin Plant Modification Proposals for new / non-routine feeds to SIXEP. This modelling route is also endorsed within the FGMSP Effluent Strategy
- Investigation of mechanisms – initial Cs breakthrough vessel performance trends; bed history; sudden and unexpected high Sr-90 discharge peak was shown to be caused by an incorrectly caustic dosed FHP skip, where Na⁺ levels exceeded 500 ppm.
- Short-term forecasts.
- Model output in form of discharge profiles (directly comparable to plant data), but also bed loading profiles, lead bed discharge predictions and competing ion elution profiles
- Modelling has underpinned requirement for improved monitoring and feed sampling.

Conclusions

The challenge of establishing a predictive understanding of an industrial process such as SIXEP requires modelling techniques from the molecular to bulk process scale. A collaborative technical approach between NNL chemical and process modellers, experimental effluent scientists and Sellafield customer plant technologists has resulted in a model that is accurate and reliable, and is used on a routine basis to predict the effect of future proposed effluent challenges to one of Sellafield’s most important plants. The attention to developing a mechanistic understanding has not only led to the model being robust, but to the science being used to build models of other processes and plant on the Sellafield site. A remaining (ongoing) challenge is to coordinate the linking of information flowing between the detailed mechanistic models and the higher level throughput

and strategy models, in terms of improved learning through R&D and the capturing of analytical and process data, such that the combined modelling suite are based on the same up to date information and therefore providing the greatest support to the Sellafield retrievals and decommissioning programmes

Acknowledgements

We would like to acknowledge the support of Sellafield Ltd, both financially and technically in the development of this work – particularly Simon Kellet and Peter Rand. We would also like to acknowledge our academic collaborators over many years in this area – who have helped to direct our understanding of these processes.

References

1. A. Dyer, J. Newton, L. O’Brien, S.L. Owens, *Zeolite, Microporous and Mesoporous Materials*; **120**, 272, (2009).
2. A. Dyer, J. Newton, L. O’Brien L, S.L. Owens, *Zeolite, Microporous and Mesoporous Materials*, **117**, 304, (2009).
3. “Modelling and simulation in the nuclear industry”, V.B. Ashley, R.B. Jarvis, S.L. Owens, *The Chemical Engineer* – September Edition (2006).
4. “User’s Guide to PHREEQC Version 2 – A Computer Program for Speciation, Batch Reaction, One-Dimensional Transport and Inverse Geochemical Calculations”, Parkhurst, D.L. and Appelo, C.A.J., US Geological Survey, Water-Resources Investigations Report 99-4259.
5. “MTDATA - Thermodynamics and Phase Equilibrium Software from the National Physical Laboratory”, Davies R H, Dinsdale A T, Gisby J A, Robinson J A J, Martin S M, *CALPHAD*, **26**, 229, (2002).
6. “Computer Simulation of Liquids” by M. P. Allen, D. J. Tildesley (ISBN-13: 978-0198556459) gives a very good summary of the technique and its use.
7. L.L. Ames Jr., *Amer. Miner.*, **45**, 689, (1960).
8. M. Johnson, D. O’Connor, P. Barnes, C. R.A. Catlow, S.L. Owens, G. Sankar, R. Bell, S.J. Teat, R. Stephenson, *J. Phys. Chem. B*, **107**, 942, (2003).
9. F.M. Higgins, N. H. de Leeuw, S.C. Parker, *J. Mater. Chem.*, **12**, 124, (2002).
10. Z. Maher, PhD Thesis, “The treatment of colloids formed in the processing of radioactive wastes” University of Manchester, (2012).

NEPTUNIUM EXTRACTION IN AN ADVANCED PUREX PROCESS AND THE EURO-GANEX PROCESS

Mike Carrott, Colin Gregson and Robin Taylor

robin.j.taylor@nnl.co.uk

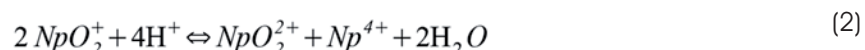
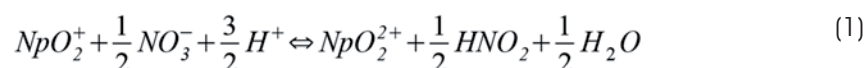
This report summarises the results of two separate but related studies of neptunium process chemistry recently completed by NNL[1-2]. Firstly, we describe the testing of a flowsheet designed to fully extract neptunium with uranium and plutonium in the first stage of an Advanced PUREX process (using tributyl phosphate, TBP, diluted in odourless kerosene, OK, as the solvent). Secondly, neptunium behaviour in the same stage (primary extract-scrub contactor) of the so-called EURO-GANEX process is described. The EURO-GANEX process uses a different extracting ligand (tetraoctyl diglycolamide, TODGA) and is designed to co-recover all transuranic actinides from neptunium to curium for recycling in a fast reactor. PUREX and GANEX processes (or variations thereof) represent the two main options under development within Europe for future aqueous reprocessing of thermal and fast reactor oxide fuels. These processes cover the spectrum of options for recycling of both major (U,Pu) and minor (Np,Am,Cm) actinides in either heterogeneous or homogeneous loading scenarios.

Introduction

Neptunium (Np) in the nuclear fuel cycle is an issue of concern since ^{237}Np is present in significant quantities in spent nuclear fuels, has a 2.1 million year half life and, due to the stability of the pentavalent neptunyl ion (NpO_2^+), can be mobilised in the environment under certain conditions. Current practice in nuclear fuel reprocessing is to treat Np as a waste and to purify uranium (U) and plutonium (Pu) products from Np, which is then routed to high level wastes for vitrification. Alternatively, recovery and recycling of Np, probably incorporated into (U,Pu) mixed oxide fuels, is an option. Indeed, in the past Np has been recovered for ^{238}Pu production by adding specific additional separation stages to existing reprocessing plants.

In current reprocessing flowsheets, Np is split between different product and raffinate streams; one impact being that an additional solvent extraction cycle is required to decontaminate U from Np. It has also been implicated as a corrosion accelerator in some waste storage tanks and evaporators. Therefore, improved control of Np in advanced reprocessing plants can reduce the complexity and hence costs of reprocessing by elimination of some process steps. Additional perceived benefits to the fuel cycle if Np is recycled into (U,Pu) fuels are removal of Np from high level waste and added proliferation resistance, although this will be at the expense of additional complexity in fuel manufacturing.

The splitting of Np between different streams in reprocessing is due to speciation as Np can exist in several inter-convertible oxidation states in solution. Np speciation in nitric acid is governed by the equilibrium established between Np(V) and Np(VI) (given in Eq. (1)) and the rates of the forward and reverse reactions. The most interesting feature of this reaction is the dual role of nitrous acid (HNO_2), which reduces Np(VI) to Np(V) but at low concentrations catalyses the oxidation of Np(V). This leads to a complex system with the kinetics and equilibria of this reaction in nitric acid solutions having been studied by many researchers over the last 60 years. At high acidities Np(V) also disproportionates into Np(VI) and Np(IV) ions – Eq. (2).



Neptunium behaviour in the PUREX process

Current reprocessing plants use the PUREX process in which pure U and Pu products can be recovered from dissolved spent fuel solution using solvent extraction between nitric acid and 30 % TBP/OK (tributyl phosphate diluted in odourless kerosene). However, the PUREX process is not ideal for recovering Np since Np(V) has a very low extractability into 30 % TBP/OK whilst Np(VI) has a rather high extractability and Np(IV) is moderately extractable depending on the conditions.

So, Np process chemistry in the PUREX process is complex and influenced by nitric and nitrous acid concentrations, U solvent loading (i.e. free TBP concentration), temperature, radiation, contactor residence times and any other redox-active ions present in or added to dissolved spent fuel solutions.

The key to controlling Np in reprocessing is really to ensure complete extraction of Np as either IV or VI oxidation states in the primary extraction section (without addition of any process reagents that affect the behaviour of U and Pu or add to the high level waste). After this selective complexation of Np(IV) or reduction of Np(VI) is effective at routing Np to a specific stream. Basically, this requires careful manipulation of the equilibrium reaction Eq. 1, which is a very difficult task, particularly so if centrifugal contactors, in which residence times may be less than the timescales required for the reaction to go to completion, are to be used.

Nevertheless, despite such complexities and following lab scale kinetic experiments and runs using a single centrifugal contactor stage,>NNL recently showed in a flowsheet test that full recovery of Np is possible in an Advanced PUREX process using centrifugal contactors simply by optimising conditions in the primary extraction and scrub contactors; this will be described in the next section.

Neptunium extraction in an Advanced PUREX process

Description of flowsheet

A miniature 14-stage centrifugal contactor cascade, housed in a Central Laboratory fumehood, was arranged as shown in Fig. 1 to represent the primary extract and scrub sections ("HA/HS") of a PUREX process with the solvent product (SP1) exiting the cascade at stage 1 and the aqueous raffinate (AR1) at stage 14. Some sections were heated to ~50 °C and NaNO₂ was added in the extract contactors (simulating radiolytically generated HNO₂ in a dissolved spent fuel solution). The active feed (HAF) was prepared by combining stock solutions of uranyl nitrate, Np and NaNO₂. The Np stock solution was pre-conditioned electrochemically to Np(V), which represented the most pessimistic situation.

Specific procedures were used to run up the flowsheet to a steady state position, monitored by on-line spectrophotometric analysis of the U concentration in SP1. Small inter-stage samples were taken periodically from the first contactor of the extract section (HA1) and analysed for HNO₂. At approximately one hour intervals during the trial, the rotor speeds, flow rates and temperatures were measured and samples of the AR1 and SP1 products were taken for off-line analysis:

- Np by γ -spectroscopy or α -spectrometry
- U by spectrophotometry
- aqueous and solvent phase acidities by titration using the potassium fluoride method
- HNO₂ by a colorimetric method based on forming an azo-dye

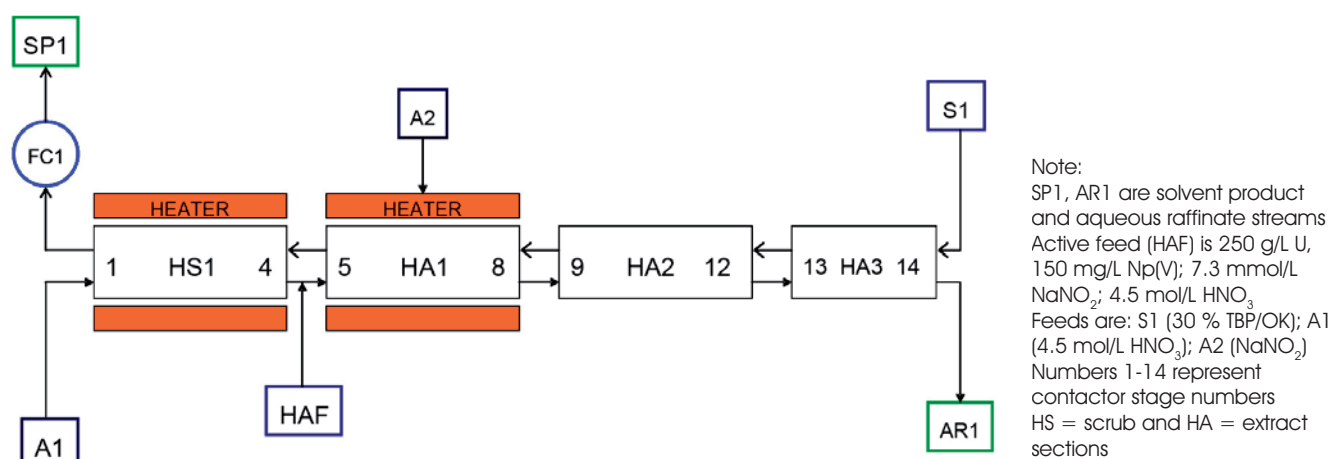


Figure 1: Neptunium extraction flowsheet tested (first section of an Advanced PUREX process)

Results of the flowsheet test

On-line spectrophotometric monitoring showed that a steady state U concentration of ~ 80 g/L in SP1 was attained after ~ 90 minutes run up. Off-line analysis showed good agreement with the on-line analysis. Np reached a steady state concentration of around 56–58 mg/L in SP1 after 3 hours run time. Good average mass balances were obtained, with that of U calculated to be 101.0 % and 101.5 % for Np. U remaining in the aqueous product was below the limit of detection for electronic absorption spectroscopy (EAS), confirming the expected excellent extraction of U ($\gg 99$ %). The results also showed that the concentration of Np in the aqueous product was very low (0.5–2 mg/L), close to the limit of detection. An average value of ~ 0.8 % Np was calculated to be routed to AR1.

At the end of the trial, profile samples across the 14 stages (aqueous and organic phases) were analysed. From the Np solvent profile (Fig. 2) it is evident that Np(V) oxidation and extraction occurs over stages 5 to 9, as shown by the increase in the Np concentration in the solvent from 3 mg/L at stage 9 to 65 mg/L at stage 4. After stage 9 the Np concentration in the solvent falls below 1 mg/L and at this point is probably below the limit of detection for the analytical method. The aqueous profile shows that rapid oxidation and extraction of Np occurs in HA1, as the concentration falls from 116 mg/L (stage 5) to < 1 mg/L (stage 9).

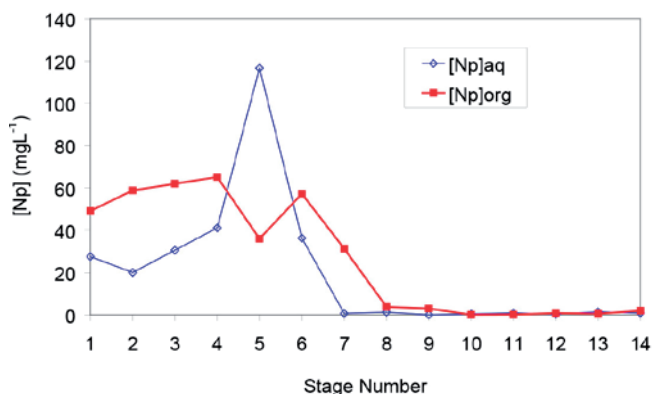


Figure 2: Neptunium aqueous and organic phase profiles across the contactor

Discussion

In the isolated aqueous phase the equilibrium position of Eq.(1), Np(V)/Np(VI) ratio, is established by the $\text{HNO}_3/\text{HNO}_2$ ratio and can be understood in terms of the equilibrium constant of Eq.(1) and its endothermicity [3]. Therefore, higher HNO_3 concentrations, lower HNO_2 concentrations and elevated temperatures increase the steady state concentration of Np(VI). However, at HNO_2 concentrations below 0.1 mmol/L this equilibrium is not easily reached (long timescales), because HNO_2

is required to catalyse the oxidation of Np(V). In 5 mol/L HNO_3 a maximum rate of oxidation is reached at ~ 1 mmol/L $[\text{HNO}_2]_{\text{initial}}$ at 50 °C although this is known to be dependent on the ratio $[\text{HNO}_2]/[\text{Np(V)}]$. In a 2-phase system similar trends are observed but with some subtle variations due to the extraction of HNO_2 into the solvent phase, which reduces the aqueous phase concentration available to catalyse the Np(V) oxidation reaction by a factor of ~ 10 . Also, as the Np(VI) product is extracted into the solvent phase, the Np(V)/Np(VI) equilibrium positions are changed.

These data suggested that conditions in the aqueous phase of around 4-5 M HNO_3 and 50 °C in the low U stages, where most of the oxidation will occur, should maximise the rate of oxidation of Np(V) in the flowsheet providing an optimum concentration of HNO_2 (or $[\text{HNO}_2]/[\text{Np(V)}]$ ratio) can be maintained in the aqueous phase. A flowsheet was consequently designed and tested in a centrifugal contactor cascade. This test successfully demonstrated that > 99 % Np can be extracted in the first (HA/HS) contactor of an Advanced PUREX process even in short residence time centrifugal contactors. This test is expected to be conservative compared to reprocessing spent fuel solutions since the HAF was conditioned to Np(V) – any storage post-dissolution would decrease the initial Np(V)/(VI) ratio – and HNO_3 radiolysis would provide a fairly constant supply of HNO_2 across the contactor with spent fuel solutions, this being available to promote Np(V) oxidation across more extract stages than in this simulant test. This work thus represents a significant step forward in the development of an Advanced PUREX process.

Further work

We are currently working with the Universities of Lancaster and Manchester to develop models of Np chemistry. Specifically, at the University of Lancaster we are collaborating on kinetic modelling of Eq. (1) – the Np(V)/(VI) redox equilibrium reaction – to try and obtain a fundamental description of the reaction mechanism. The University of Manchester, via an EPSRC Impact Acceleration Award, are developing a process model of the NNL flowsheet using gPROMS software so it will be fully compatible with our own solvent extraction modelling capability. Results from the modelling studies are expected to be published shortly.

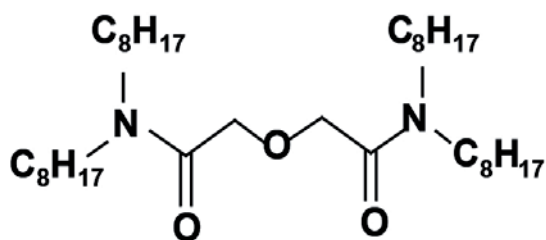
This HA/HS flowsheet now needs to be coupled to the subsequent flowsheet section in which we envisage a co-(U,Pu,Np) product is separated from the bulk mass of U, which is then backwashed into dilute nitric acid. Ultimately, the goal is to test the complete design of an Advanced PUREX process using spent fuel solution (a 'hot' test) in the Phase 3 High Active (HA) cells of NNL's Central Laboratory in order to demonstrate a much rationalised and more proliferation resistant

reprocessing flowsheet that meets the requirements for a sustainable, closed nuclear fuel cycle in the 21st Century!

The EURO-GANEX process

For the homogeneous recycling of mixed actinides in fast reactor fuels, the concept for a Grouped Actinide Extraction (GANEX) process is under development in Europe. This is expected to involve two solvent extraction cycles, firstly removing the bulk uranium and then recovering the transuranic (TRU) elements in a 2nd TRU cycle. As part of the European 7th Framework Programme (FP7) funded "ACSEPT" project the so-called EURO-GANEX process was developed; this uses a combination of TODGA (N,N,N',N'-tetraoctyl diglycolamide) and DMDOHEMA (N,N'-(dimethyl-N,N'-dioctylhexylethoxy-malonamide) in odourless kerosene (OK) as the organic phase (Fig. 3). In a parallel situation as described for the Advanced PUREX process, a specific concern in developing the GANEX flowsheet was the full extraction of neptunium ions in the primary extract and scrub contactor. Indeed, in a flowsheet trial using the glove box housed centrifugal contactor rig in NNL's PuMA Labs only ~70 % of neptunium had been extracted in the primary extract and scrub section compared to >99.99 % of the plutonium and americium. As there was relatively little knowledge on neptunium chemistry in diglycolamide or malonamide based solvents in the literature, some basic studies were made by NNL to better understand neptunium behaviour in the process. These studies are summarised in the next section.

(a)



(b)

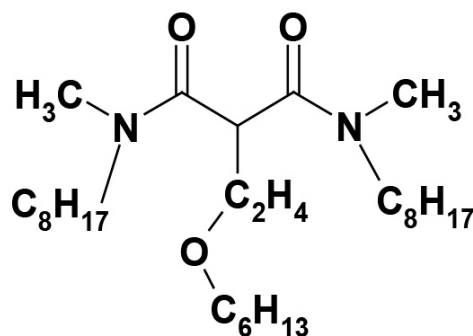


Figure 3: Structures of a) TODGA and b) DMDOHEMA ligands

Neptunium extraction and stability in the GANEX solvent phase

Experiments

Three solvent phases were used: (a) the "GANEX solvent": 0.2 mol/L TODGA + 0.5 mol/L DMDOHEMA in OK; (b) 0.2 mol/L TODGA in OK and (c) 0.5 mol/L DMDOHEMA in OK. ²³⁷Np stock solutions were electrochemically conditioned to generate specific solutions of Np(IV), Np(V) and Np(VI) so that the reactions of each individual oxidation state could be followed. Batch distribution experiments were used to determine distribution ratios ($D_M = [M]_{\text{organic}}/[M]_{\text{aqueous}}$) by solvent extraction of Np from nitric acid into the organic phase followed by γ -spectroscopy of each phase. UV/vis/NIR spectrophotometry (EAS) was used to follow the stability of Np oxidation states in the organic phases after extraction. Interpretation of spectra in these organic phases was quite complex. Some reference spectra are shown in Fig. 4(a-b) for Np(IV) and Np(VI) in TODGA and DMDOHEMA phases as well as how the Np(VI) spectrum in DMDOHEMA varied with HNO₃ concentration (Fig. 4(c)). Spectra in the GANEX solvent phase were basically additives of the independent TODGA and DMDOHEMA spectra. The spectra were shown to adhere to the Beer-Lambert law across the Np concentration ranges used.

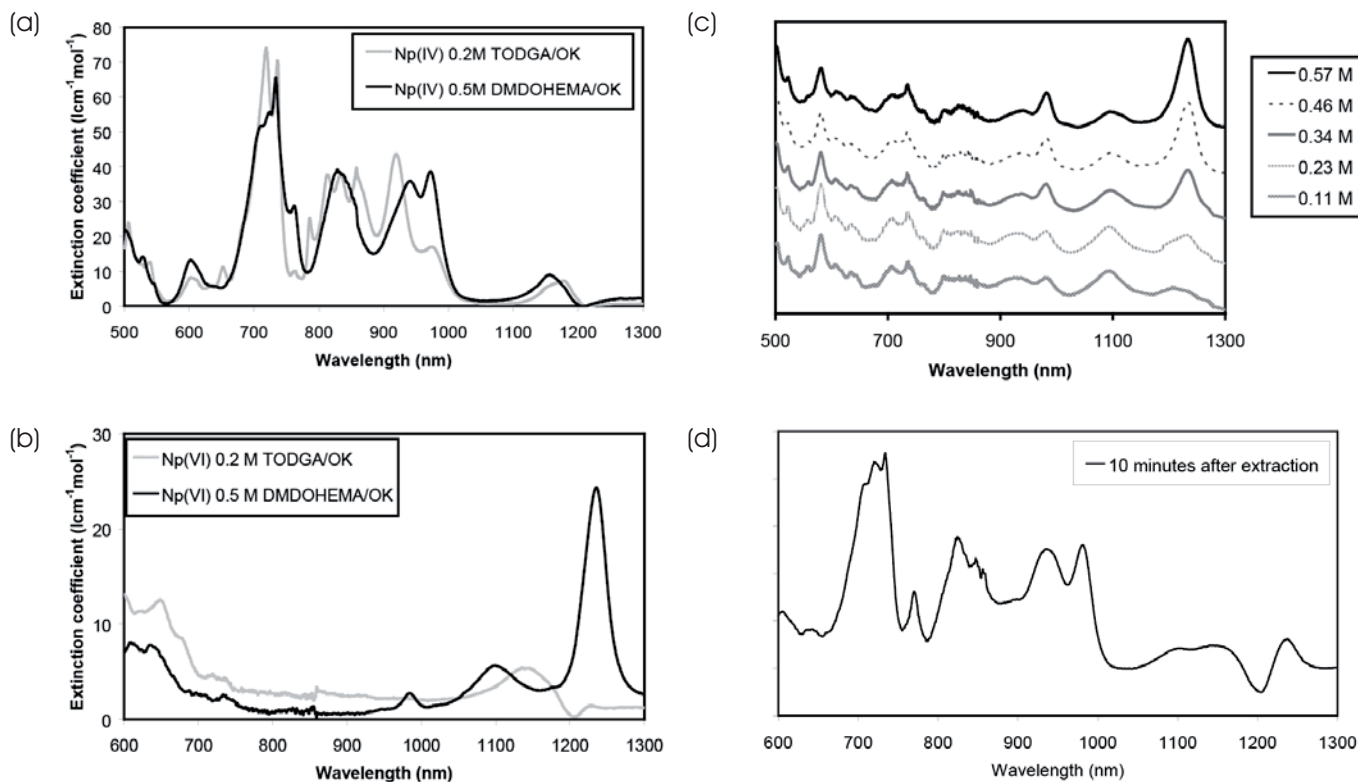
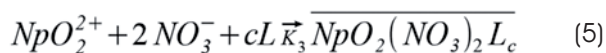
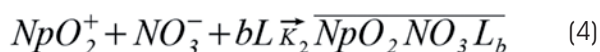


Figure 4: Organic phase EAS in 0.2 mol/L TODGA/OK and 0.5 mol/L DMDOHEMA/OK after extraction from 5 mol/L HNO₃ for (a) Np(IV) and (b) Np(VI); (c) Np(VI) organic phase EAS with varying equilibrium [HNO₃]_{org} in 0.5 mol/L DMDOHEMA/OK; (d) EAS of the organic phase recorded after extraction of Np(V) from 5 mol/L HNO₃ into the GANEX solvent and phase separation

Extraction chemistry

From Fig. 5(a) it can be seen that the order of extractability into the GANEX solvent follows: Np(IV) >> Np(VI) >> Np(V). Fig. 5(b) shows the corresponding extractabilities of Np(IV) and Np(VI) ions in the separate solvents, *i.e.* 0.2 mol/L TODGA/OK and 0.5 mol/L DMDOHEMA/OK. Simplistically, extractions into DMDOHEMA or TODGA or the GANEX solvent mixture can be described by Eq. (3-5) where L = TODGA or DMDOHEMA.



Values of *a-c* for the ligand L were calculated from the gradients of *logD* vs. *log[L]* plots and data for separate solutions of TODGA and DMDOHEMA with Np(IV) and Np(VI) ions are summarised in Table 1.

These results indicate that, after extraction from 1 mol/L HNO₃, 2 tridentate TODGA molecules and 4 bidentate DMDOHEMA molecules complex Np(IV) and 2-3 TODGA and 3 DMDOHEMA molecules complex Np(VI). Assuming the nitrate ions required for charge neutralisation in the organic complex are bidentate this would imply unusually high coordination numbers. As HNO₃ concentration increases there is a decrease in the solvation numbers for Np(VI) to 1 TODGA and 1-2 DMDOHEMA ligands at 4 mol/L HNO₃ (aqueous phase acidity). Explanations in the literature are that some nitrate ions are monodentate or that the extractants either have a lower denticity or some ligands are outer sphere coordinated; aggregation in the organic phase is a further possibility. Corresponding data for Np(IV) were difficult to obtain due to very efficient extraction of Np(IV) above 1 mol/L HNO₃ and problems with third phase formation. However, the solvation numbers appeared to increase between 0.5 and 1 mol/L [HNO₃]_{aq}.

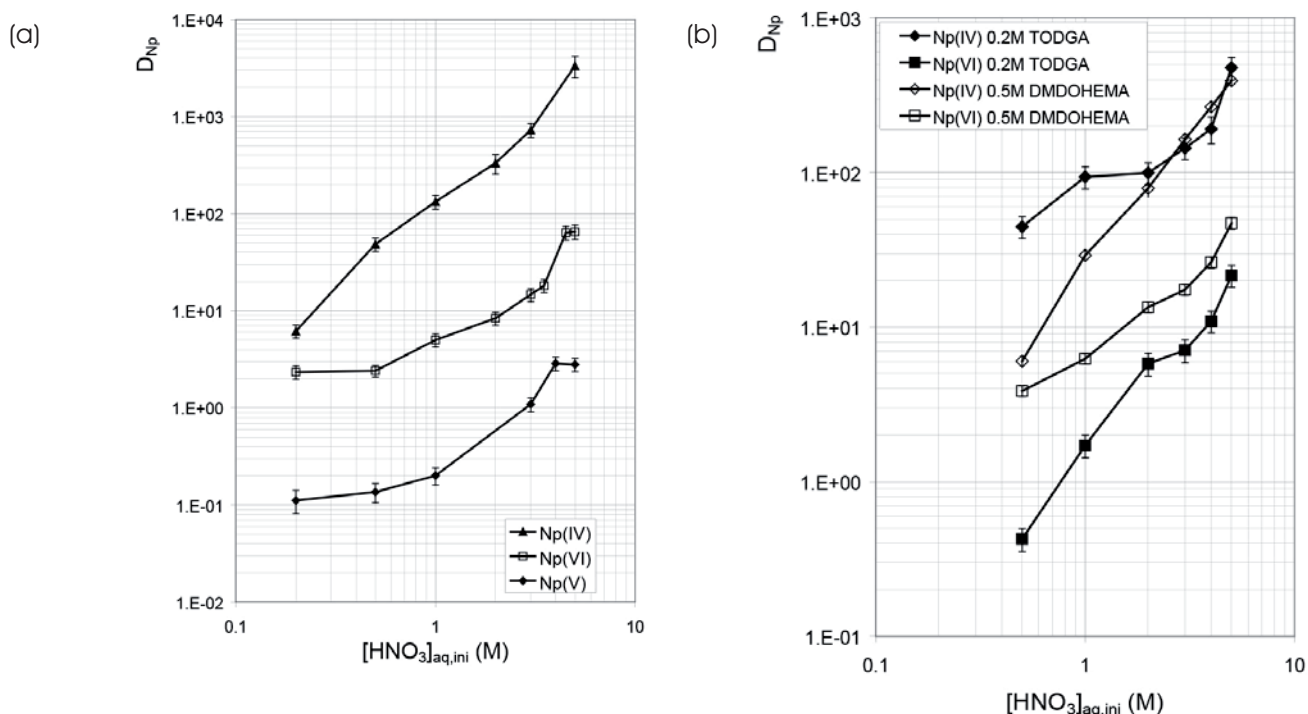


Figure 5: a) Distribution ratios for Np(IV), Np(V), Np(VI) ions extracted into the GANEX solvent (0.2mol/L TODGA / 0.5 mol/L DMDOHEMA/OK) and (b) distribution ratios for Np(IV) and Np(VI) ions extracted into separate 0.2 mol/L TODGA/OK and 0.5 mol/L DMDOHEMA/OK solvents (error are ± 2)

Table 1. Solvation numbers for extractions of Np(IV) and Np(VI) ions into separate TODGA/OK and DMDOHEMA/OK phases from aqueous nitric acid (* indicate data reported by Ansari et al. *Solv. Extr. Ion Exch.* v.30, p. 457, 2012)

Oxidation State	$[HNO_3]_{aq,eqm}$ (M)	Extractant	Solvation Number (± 2)
Np(IV)	0.5	TODGA	1.8 ± 0.0
Np(IV)	1	TODGA	2.0 ± 0.1
Np(IV)*	3	TODGA	2.22 ± 0.15
Np(VI)	0.5	TODGA	2.4 ± 0.3
Np(VI)	1	TODGA	2.4 ± 0.5
Np(VI)	2	TODGA	1.8 ± 0.1
Np(VI)*	3	TODGA	1.38 ± 0.08
Np(VI)	4	TODGA	1.1 ± 0.1
Np(IV)	0.5	DMDOHEMA	2.3 ± 0.5
Np(IV)	1	DMDOHEMA	4.1 ± 0.5
Np(VI)	0.5	DMDOHEMA	2.9 ± 0.3
Np(VI)	1	DMDOHEMA	2.9 ± 0.2
Np(VI)	2	DMDOHEMA	2.6 ± 0.1
Np(VI)	4	DMDOHEMA	1.6 ± 0.1

Stabilities of Np ions in the GANEX solvent

As it is well known that Np oxidation states inter-convert dependent on solution conditions and that rates of redox reactions in organic phases vary from those in aqueous phases we studied the stability of the various oxidation states in the GANEX solvent.

EAS of Np(IV) extracted from 5 mol/L HNO_3 into the GANEX solvent showed that Np(IV) is stable for > 16 hours. Np(VI) extracted from 5 mol/L HNO_3 into the

GANEX solvent showed a slow reduction over ~ 19 hours. It was concluded that Np in these oxidation states will be sufficiently stable within a solvent extraction process using short residence time centrifugal contactors. More interestingly, in the GANEX solvent Np(V) was found to be quite unstable with substantial Np(IV) and Np(VI) clearly present in the first separated organic phase spectrum taken after mixing with an aqueous phase containing Np(V) in 5 mol/L HNO_3 (Fig. 4(d)). Np(IV) peaks then showed a gradual increase on standing. A mass balance exercise was carried out to determine the quantities of Np(IV) and Np(VI) generated following extraction. The results showed that a good mass balance is obtained with equal concentrations of Np(IV) and Np(VI) formed, thus indicating that solvent phase disproportionation (Eq. (2)) is the cause of Np(V) instability at high acid concentrations. In an earlier study we have measured the kinetics of Np(V) disproportionation in TBP solutions showing

that it is more rapid in the organic than in the aqueous phase [4]. Given the rather high concentrations of HNO_3 that can be extracted by the GANEX solvent, this rapid disproportionation is not unexpected.

Discussion

Given the high distribution ratios for Np(IV) and Np(VI) and the quite rapid disproportionation of Np(V) high acid conditions within a GANEX solvent extraction

flowsheet should lead to full extraction of Np, whatever its initial redox speciation in the aqueous feed. However, decontamination of some partially extractable fission and corrosion products requires low acid scrub conditions, so the combination of adjacent high acidity extract and low acidity scrub sections could lead to accumulation of Np or other species across the contactor with a risk of exceeding the loading capacity of the solvent and forming a third phase. Therefore, the design of the extraction section of the GANEX flowsheet needed to be a compromise between optimising Np extraction and minimising fission product contamination of the organic phase, without risking third phase formation or compromising recoveries of Pu and Am/Cm. Based on the surrogate feed test at NNL, modelling at CEA Marcoule (a partner in the ACSEPT project), using their PAREX solvent extraction code, and the experimental data we generated on Np, a flowsheet was designed and tested with spent fuel solution at the Joint Research Centre Institute for TransUranium elements (JRC-ITU, Karlsruhe, Germany) right at the end of the ACSEPT project. This report will not describe the results of the JRC-ITU 'hot' test other than to point out that >99.9 % Np was recovered from the primary extract-scrub contactor (noting also that short residence time centrifugal contactors were used for this test). It seems likely that this excellent, but rather surprising, result was due to two factors; both promoted at higher acidities and elevated temperatures:

- Np(V) disproportionation in aqueous and organic phases via Eq. (2)
- Np(V) oxidation to Np(VI), catalysed by radiolytically generated nitrous acid via Eq. (1)

Further work

Whilst the work to date was sufficient to aid the design of the EURO-GANEX flowsheet, determination of the kinetics of Np(V) disproportionation and Np(VI) reduction in TODGA and DMDOHEMA organic phases is of fundamental interest and also will be needed for process modelling. Additionally, the contribution to Np extraction in the hot test due to Np(V) oxidation by nitric acid (Eq. (1)) needs to be evaluated in similar experimental and modelling studies as have been made for the Advanced PUREX process. These basic data would enable us to thoroughly underpin Np extraction in the primary section of the EURO-GANEX process flowsheet.

Conclusions

In the development and design of solvent extraction processes for advanced aqueous based reprocessing of spent thermal and fast reactor oxide fuels, the control of Np is a key challenge to address. In particular, in the first extraction section it is difficult to fully extract Np into

the organic phase, especially if short residence time centrifugal contactors are to be used. This is due to the fact that Np can exist in three different oxidation states in nitric acid that are easily inter-convertible by reactions with $\text{HNO}_3/\text{HNO}_2$ or disproportionation/reproportionation and which have differing affinities for extraction into organic phases. In our work developing Advanced PUREX and GANEX process flowsheets, common issues regarding Np behaviour were encountered. Our experience is that understanding the basic redox chemistry in aqueous and organic phases and distribution into the solvent phase, coupled with single stage and multi-stage centrifugal contactor trials, underpins successful flowsheet design. It has consequently been shown that >99 % Np can be recovered in Advanced PUREX and GANEX flowsheet tests giving confidence that targets, with regards to Np recycle, for future closed fuel cycles can be met.

Acknowledgments

The authors acknowledge the many contributions over the last decade or more from past and present team members and other NNL colleagues to our neptunium extraction studies. The work described herein has been supported by the UK National Nuclear Laboratory's Signature Research Programme in Spent Fuel and Nuclear Materials and the European Union Framework 7 Programme "ACSEPT" project (FP7-CP-2007-211267).

References

1. R.J. Taylor, C.R. Gregson, M.J. Carrott, C. Mason, M.J. Sarsfield, "Progress towards the full recovery of neptunium in an advanced PUREX process", *Solvent Extraction and Ion Exchange*, **31**, 442, (2013).
2. M.J. Carrott, C.R. Gregson, R.J. Taylor "Neptunium extraction and stability in the GANEX solvent: 0.2 M TODGA / 0.5 M DMDOHEMA / kerosene", *Solvent Extraction and Ion Exchange*, **31**, 463, (2013).
3. C.R. Gregson, C. Boxall, M.J. Carrott, S. Edwards, M.J. Sarsfield, R.J. Taylor, D. Woodhead, "Neptunium (V) Oxidation by Nitrous Acid in Nitric Acid", *Procedia Chemistry*, **7**, 398, (2012).
4. M.J. Sarsfield, R.J. Taylor, C.J. Maher, "Neptunium(V) disproportionation and cation-cation interactions in TBP/kerosene solvent", *Radiochimica Acta*, **95**, 677, (2007)

DENSITY FUNCTIONAL THEORY CALCULATIONS OF THE ACTINIDE (VI) / ACTINIDE (V) REDOX POTENTIALS IN WATER

Helen M. Steele, Dominique Guillaumont ^a and Philippe Moisy ^a

helen.steele@nnl.co.uk

Introduction

Some of the most unique ions in the actinide series are the actinyl (V) ions $\{\text{AnO}_2^+\}$, which contain two strongly bound oxygen atoms in a linear $\text{O}=\text{An}^+=\text{O}$ arrangement resulting in a small effective positive charge on the metal. As a result the actinyl (V) ion is very soluble, does not easily hydrolyse at environmental pHs and can only interact weakly with most minerals leading to increased mobility. This behaviour is particularly evident in neptunium chemistry.

The actinyl (VI) ion $\{\text{AnO}_2^{2+}\}$ has the same structure but with a higher effective charge on the metal ion. The stability of the actinyl (V) ion depends on the redox couples between its An(IV) and An(VI) states.



Here we focus on the actinyl (VI/V) redox couple. Complexation, environmental and chemical conditions can alter the magnitude of an element's redox potential, increasing the uncertainty in predicting and controlling that element's mobility. If we are going to have improved control over difficult and highly mobile elements such as neptunium it is necessary to be able to accurately and consistently measure the magnitude of a given redox potential under a range of conditions.

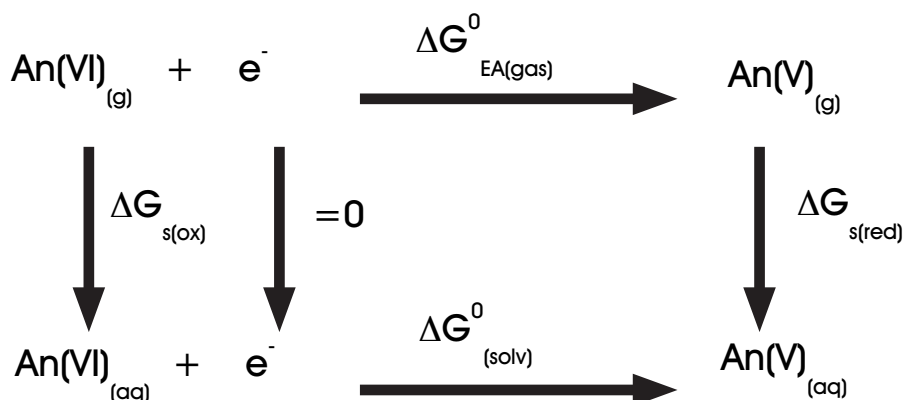


Figure 1: Gibbs free energy diagram used to calculate actinyl redox potentials as described by Hay et al. [2]

Previously the disparity between theoretical calculations and experimental measurements for the actinyl redox couples, even at the highest computational levels, has made their application in this field limited. Accordingly a program of research has been undertaken to derive a methodology to enable more accurate calculation of actinide redox potentials, which can then be applied to a range of aqueous and organic actinide systems. This paper reviews a newly derived methodology using quantum mechanics [1] to calculate actinyl redox potentials and compares the results derived to experimentally measured values [1].

For actinide systems, the accurate theoretical calculation of redox potentials remains technically challenging. This is due in part to the complexity of the electrochemical process, the size of the chemical system, and the necessity of thermodynamic accuracy. These challenges are exacerbated due to the large number of

^a Commissariat à l'énergie atomique et aux énergies alternatives

electrons, a characteristic of actinide systems for which electron correlation and the effects of relativity must be included in the calculation.

The electrochemistry of the actinyl moiety $\text{AnO}_2(\text{H}_2\text{O})_5^{2+/+}$, where An = U, Np, and Pu, was first investigated theoretically over a decade ago by Hay et al. [2] using a free-energy type cycle (Fig. 1).

For the free energy cycle shown in Fig. 1, $G_s(\text{ox})$ and $G_s(\text{red})$ are the solvation energies of the structurally and electronically oxidised and reduced species respectively; $G_{\text{EA}(\text{gas})}^0$ is the electron affinity, calculated as the change in energy in forming the reduced species at the same geometry as the oxidised species and is typically accompanied by vibrational excitation; with vertical electron transfers being the most probable type of electron transfer. Redox potentials calculated using such a free energy cycle have similar contributions in magnitude from the electron affinity and the solvation energies of both the oxidised and reduced complexes.

Using the energy cycle in Fig. 1 the total energy of the redox reaction is calculated as in Eq. (1):

$$(1) \quad G_{(\text{solv})}^0 = G_{s(\text{ox})} + G_{\text{EA}(\text{gas})}^0 + G_{s(\text{red})}$$

Where $G_{(\text{solv})}^0$ is the energy of the full redox reactions. To take an element from its ground state oxidised form $\text{AnO}_2(\text{H}_2\text{O})_5^{2+}$ to its ground state reduced form $\text{AnO}_2(\text{H}_2\text{O})_5^+$ there are three energy steps. Firstly, the structural rearrangement of the complex including the solvation energies of the $\text{AnO}_2(\text{H}_2\text{O})_5^{2+}$ species in preparation for the electron transfer; secondly, the energy of the electron transfer and thirdly, the energy required to reorganise the ligands (in this case H_2O) and the molecules of bulk solvation around the reduced actinyl to obtain a new ground state structure. The time resolution of standard experimental electrochemical techniques such as cyclic voltammetry is inadequate to determine to what extent structural and solvent rearrangement occurs; before or after the electron transfer process. It is this potential disparity in the partitioning of the energy between calculated values and those made at electrode surfaces that could lead to significant error when comparing theory and experiment.

The structural reorganisation of the reduced aqueous actinyl ions, following electron transfer, are a combination of fast and slow processes, including reorganisation of the strongly bound actinyl oxygens ($\text{O}=\text{An}=\text{O}$) and of the more weakly bound equatorial ligands, ($\text{H}_2\text{O} \cdots \text{An}$) plus reorganisation of the bulk water molecules of solvation. Such a range in bond strengths would be expected to have different time frames, and combined with the effects of mass transfer and diffusion at the electrode, the time dependence of the experimental events is difficult to ascertain. To

improve the calculation of redox potentials using a fully quantum mechanical approach we investigated the structural reorganisation and solvation energy of the actinyl species during the redox process; the effect of theoretical approach, such as the degree of electron exchange within density functionals; the role of first and second solvation shells and the necessity of corrections to the electron affinity energy, such as those for spin-orbit coupling and electron multiplet effects.

Following on from initial research we modified the theoretical approach originally reported by Hay et al. for actinyl redox calculations. Below we present a brief explanation of the key differences in our approach and the results obtained.

Theoretical approach

The calculated overall Gibbs free energy is obtained using a similar free energy cycle approach to that shown in Figure 1 but the redox potentials have been calculated non-adiabatically and do not include the energy contributions from structural reorganisation of the reduced $\text{AnO}_2(\text{H}_2\text{O})_5^+$ species, (the solvation energy of the reduced complex is calculated at the geometry of the oxidised complex). The large correction for electron multiplet effects, which has previously been included in an *ad hoc* fashion, is not included here but changes to orbital energies as a result of spin-orbit coupling have been included. A density functional theoretical approach has been taken. There exists a number of different density functionals, some are very well established such as the B3LYP functional, which when used here gave improved results with respect to previous calculations but we found the best experimental agreement was obtained when using the M06L functional, which does not contain any electron exchange. The results obtained are compared to standard potentials for the species $\text{AnO}_2(\text{H}_2\text{O})_n^{2+/+}$, where An = U, Np, and Pu for $n = 5, 6$, and the values obtained for $n = 5$ are subsequently compared with calculated values for $n = 4$ and 6 .

Results

Molecular structures

Before the redox energy calculations could be performed we ensured that the density functional approach taken gave good agreement with experimentally measured bond lengths. When calculated in conjunction with the solvation model, experimentally measured bond lengths were reproduced well. The error in the calculated actinyl bond $\text{An}=\text{O}$ is between 0.00 and 0.04 Å, and for the calculated $\text{An}-\text{H}_2\text{O}$ bond lengths a maximum overestimation error of 0.05 Å was obtained.

The electron affinity is calculated for the actinyl complex containing only its primary solvation shell where the linear actinyl unit is coordinated by between four and six explicit equatorial water molecules (Fig. 3 shows the structure for 5 waters). Then the solvation energies are calculated using the self consistent reaction field polarizable continuum model (SCRF) (PCM). Experimentally reported redox potentials are referenced to the standard hydrogen electrode (SHE), whereas redox potentials calculated are absolute. Accordingly, to enable comparison between experimental and theoretical calculated redox potentials a value of 4.44 V is used to correct the values back to the standard hydrogen potential.

Using this approach, which does not include energetic contributions from the reorganisation of the reduced species in solution, gives calculated redox potentials in good agreement with measured standard potential values for the three actinyl couples, in trend and magnitude.

Of the three components of the free energy cycle the solvation energies of the oxidised and reduced forms are predominantly a function of the charge and therefore relatively insensitive to the element as the charge is nearly equal. By contrast, the electron affinity part of the free energy cycle is highly element specific and largely determines the differences in redox potentials across the actinyl series (Table 2). For this to occur it shows that the highest energy occupied orbitals of the oxidised species are very similar to the reduced orbitals across the U, Np, Pu actinide series. The highest occupied molecular orbital (HOMO) on the reduced Np(V) species is shown in Fig. 4. The fact that this orbital does not sit on a bond but is an f-electron localised on the actinide centre may explain the lack of sensitivity of the redox potential to structural changes following reductions.

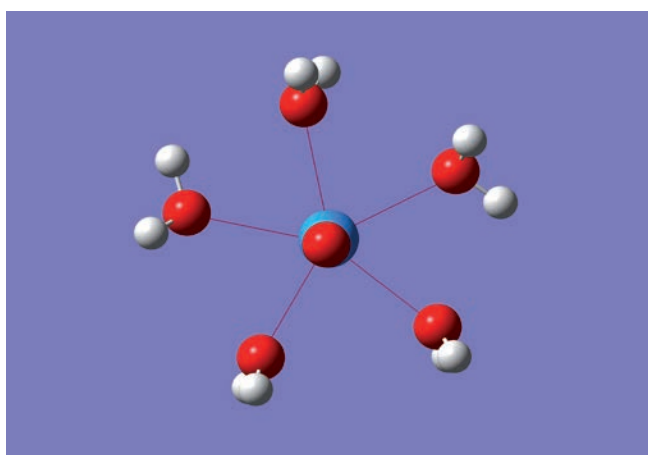


Figure 2: Structure of the $AnO_2(H_2O)_n^{2+/+}$ complex for $n=5$. The linear actinyl molecule is seen perpendicular to the plane of the water ligands

Calculated and Experimental Redox Potentials.

The calculated redox potentials for the $AnO_2(H_2O)_5^{2+/+}$ ($An = U, Np, \text{ and } Pu$) couples using the M06L density functional are given in Table 1. These values are compared with those calculated thermodynamically using the CASPT2 approach and the experimentally measured accepted redox potentials, E^0 's, are presented in the final column.

Table 1. Redox potentials calculated in the aqueous phase for $AnO_2(H_2O)_5^{2+/+}$ ($An = U, Np, \text{ and } Pu$) including the spin-orbit corrections and compared to accepted experimental values

	DFT/M06L-calculated	Previous CASPT2 [3] calculated	Standard. Measured potential E^0
U	0.136	0.00	0.088
Np	1.227	1.53	1.159
Pu	0.946	0.73	0.936
MUE*	0.04	0.22	

*Mean unsigned error

Table 2. Electron affinities calculated in the gaseous phase for the M06L DFT functionals studied and the standard measured potential E^0 's (both are normalised with respect to the Np(VI/V) couple)

	M06L Calculation	Experimental Std potential E^0
U	-1.16	-1.07
Np	0.00	0.00
Pu	-0.25	-0.22

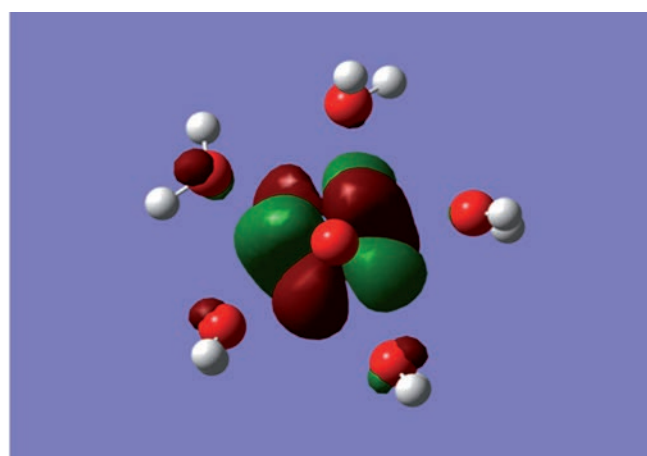


Figure 3: An illustration of the HOMO into which an electron is added on going from the Np(VI) to Np(V)

Under equilibrium conditions five is accepted as the number of water ligands around the AnO_2^{2+} ions studied here under standard equilibrium conditions, but this coordination number may not persist under highly concentrated conditions or at the surface of an electrode. The results from increasing the number of water molecules around the central actinyl ion from 4-6 on the calculated redox potentials are given in Table 3.

Table 3. Redox Potentials (V) Calculated in the Aqueous Phase for $\text{AnO}_2(\text{H}_2\text{O})_n^{2+/+}$ (An = U, Np, and Pu; n = 4–6)

	Redox potential (V)		
	U	Np	Pu
n=4	0.476	1.059	1.412
n=5	0.136	1.227	0.946
n=6	0.305	0.752	1.566

In the case of uranium and plutonium altering the number of water molecules around the central actinyl ion had an effect on the redox potential that had a minimum at n = 5, whereas for neptunium there is a maximum at n = 5.

Conclusions

The calculated redox potentials using this new theoretical approach, excluding the reorganisation energy of the reduced complex and the multiplet correction shows very good agreement, in magnitude and trend ($\text{U} < \text{Pu} < \text{Np}$) with experimentally measured values for the established standard redox potentials of the classic actinyl couples in water. This method of calculation leads to an order of magnitude improvement for calculations, which now lie within experimental error. Further it can be seen by breaking down the contributing energy parts of the free energy cycle, the electron affinity in the gas phase is directly proportional to the redox potentials. This finding has important implications in the prediction of redox properties and ultimately in furthering the understanding of actinyl oxidation state control. As well as being accurate this approach has not used any contributions from the computationally expensive vibrational energy calculations, such contributions often making the calculation of redox potentials for large systems computationally too expensive.

Acknowledgement

The authors are grateful to the CEA-Eurotalents program for funding this work and Helen Steele's secondment at CEA Marcoule.

References

1. H.M. Steele, D. Guillaumont, P. Moisy, "Density functional theory calculations of the redox potentials of actinide (VI)/actinide(V) couple in water", *J. Phys. Chem. A*, **117**, 4500, (2013).
2. P. J. Hay, R. L. Martin, G. Schreckenbach, "Theoretical studies of the properties and solution chemistry of AnO_2^{2+} and AnO_2^+ aquo complexes for An = U, Np, and Pu", *J. Phys. Chem. A*, **104**, 6259, (2000).
3. S. Tsushima, U. Wahlgren, I. Grenthe, "Quantum chemical calculations of reduction potentials of $\text{AnO}_2^{2+}/\text{AnO}_2^+$ (An = U, Np, Pu, Am) and $\text{Fe}^{3+}/\text{Fe}^{2+}$ couples", *J. Phys. Chem. A*, **110**, 9175, (2006).

MUON TOMOGRAPHY: CHARACTERISING LEGACY NUCLEAR WASTE USING COSMIC RAYS

Craig Shearer, David Mahon ^a

craig.shearer@nnl.co.uk

Introduction

Muon tomography is an innovative technology that presents significant potential benefits for the characterisation and safe long term storage of waste containers at the Sellafield site and beyond.

The technique harnesses the penetrating power of cosmic ray muons to locate and identify high-Z materials within shielded containers, passively and non-destructively, to a level that isn't possible with any other assay or characterisation method currently available.

The Muon Tomography Project is a 3-phased project that aims to take the initial concept from a small-scale prototype imaging system (Phase I) through to a full-scale 'technology demonstrator' imaging system (Phase III). The overall aim of the project is to create a fully operational industrial imaging system which can be deployed on Sellafield Ltd. sites for a variety of applications.

NNL has been funded by Sellafield Ltd. since 2009 to manage and coordinate the project, which is a collaborative effort between NNL and the University of Glasgow. This article will describe some of the basic muon science behind the images which have been obtained, as well as describing the prototype muon imaging system which is currently operational and taking experimental data at the University of Glasgow.

This article will also present some of the latest results from the imaging system which demonstrates a clear ability to differentiate high-Z materials from lower-Z material in a variety of situations (e.g. imaging the internal contents of a surrogate waste container).

Muon Production and Interactions

Muons have the same charge as the electron but are around 100 times heavier. They are routinely produced in particle accelerators around the world but by far the most abundant and easily accessible source comes from the upper atmosphere. They are short-lived and have a lifetime on the order of 10^{-6} seconds.

The Earth is under constant bombardment by high energy radiation originating from beyond the solar system which, historically, was termed cosmic rays. Cosmic rays are mainly composed of protons and atomic nuclei, and when the protons collide with nuclei in the atmosphere they produce short-lived particles called pions. These pions then decay to muons and neutrinos that continue down to sea level, where the muon flux is around $1 \text{ cm}^{-2} \text{ min}^{-1}$.

These naturally occurring muons are observed at sea level with high energies (around 3 GeV), with the number of muons decreasing as the incoming angle becomes

more acute. This high energy allows the muons to penetrate dense materials that would otherwise block or restrictively attenuate more common radiations, such as X-rays or gamma-rays. A muon with 3 GeV of energy can traverse almost 2 meters of lead before being absorbed, for example.

Multiple Coulomb Scattering

Cosmic ray muons simply pass through the majority of matter without interacting, however, for high-Z ($Z =$ atomic number) materials such as uranium (U) or lead (Pb) muons *will* interact and scatter (via Coulomb scattering).

Coulomb scattering is when a (charged) cosmic-ray muon is incident on a given material and it undergoes multiple small-angle scattering due to electromagnetic interactions with the protons in the material's nuclei. The majority (98%) of the distribution of scattering angles can be described by a regular Gaussian distribution.

^a University of Glasgow

The extent of this Coulomb scattering is dependent on the atomic number of the material; the higher the Z of the material through which the muon passes the larger the angle by which the muon will scatter. This relationship is exploited in muon tomography, to allow the imaging of objects within nuclear waste containers (e.g. ILW containers). As noted previously, conventional imaging radiations, such as X-rays are not penetrating enough for such an application.

This scattering information can then be used to identify the materials through which the muon has passed and thereby create an 'image' of the material density within the container under investigation.

Muon Imaging Techniques: Transmission and Scattering

In the 1960s L. W. Alvarez searched for hidden chambers within the Second Pyramid of Chephren in Egypt [1] using the so-called *transmission* technique. This study measured the relative flux of cosmic ray muons after they had passed through the structures of interest, in other words, the transmission technique works just like taking an X-ray. Denser materials absorb more muons whilst lighter materials and cavities absorb fewer muons and therefore a 2D image of the density structure of the interior volume can be produced.

In 2003 Borozdin *et al* [2] introduced the potential of using the multiple Coulomb scattering of muons (i.e. the *scattering* technique) for the identification of illicit high-Z materials concealed within shielded transport (ISO-freight) containers. In this approach, the measurement of the initial and Coulomb-scattered muon trajectories allows the three dimensional location of scattering objects within the structure to be determined. The *scattering density*, λ for a given material is defined in [3] and is shown in Eq. (1).

$$\lambda \equiv \left(\frac{13.6}{p_0} \right)^2 \frac{1}{X_0} \quad (1)$$

The scattering density represents the mean square scattering angle of muons with a nominal momentum p_0 travelling through unit length of the given material. We can see from Equation 1 that, as λ depends on the radiation length X_0 , high-Z materials will have larger values of λ and low-Z materials smaller values. It is this relationship which allows the identification of different materials using muon scattering information.

The collaborative R&D programme undertaken by NNL and the University of Glasgow has constructed a small-scale prototype imaging system in order to demonstrate the practical feasibility of using this scattering technique to identify high-Z materials within a sealed container. The imaging system and its performance will be described in the following sections.

The Prototype Muon Imaging System

Prior to Phase I of the project an initial Monte Carlo (modelling) feasibility study was undertaken in late November 2009 with promising results [4]. In order to validate the results of that initial study Phase I of the Muon Tomography Project produced a fully operational, small-scale, prototype muon based imaging system which has allowed the experimental validation to be undertaken.

The essential detection requirements for muon scattering tomography is the ability to measure the trajectory of a cosmic ray muon before it is scattered by a given object and to measure its trajectory after it has been scattered. This requires sensitive detection materials to be placed above and below the container to be imaged (Fig. 1).

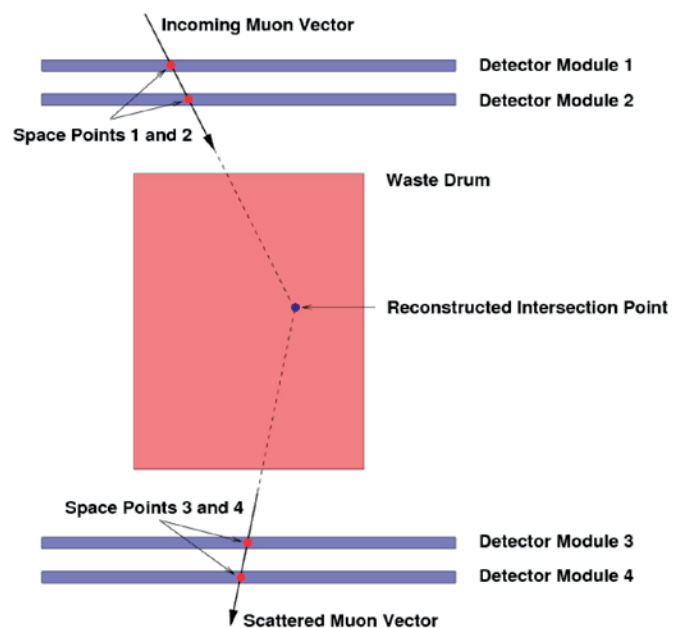


Figure 1: Schematic view of a waste drum placed in the imaging volume of the muon based imaging system

The project chose scintillating fibres as the active medium for its muon detector, due to their robustness in industrial environments. The fibres used have a diameter of 2 mm. The light emission output from this fibre choice (which peaks at 432 nm), provides excellent overlap with the sensitivity of the chosen detector, a Multi-Anode Photomultiplier Tube (MAPMT) (Fig. 2), which detects the light transmitted along the fibre that is created when an incident muon passes through the fibre.

Detailed Monte Carlo simulation studies determined that the optimum fibre width for the anticipated light output and reconstructed image resolution was 2 mm [4].

The detector consists of 4 individual detector modules (2 above the object being imaged and 2 below). Each module contains two orthogonal (perpendicular) layers of 128 fibres.



Figure 2: MAPMT detector – with the fibre connection scheme overlaid

The fibres are glued onto a low-Z support sheet that is fixed to an aluminium baseplate. The fibres are then routed to the read-out MAPMTs which have a square array of 64 pixels with 2 fibres at attached to each pixel (Fig. 2) to minimise the overall cost of the readout system, and also to reduce the quantity of electronics which are required, while not impacting on the quality of the images produced.

Fig. 3 (top) shows the initial CAD model of the prototype imaging system designed at the start of Phase I and Fig. 3 (bottom) shows the experimental prototype imaging system which is currently operating at the University of Glasgow.



Figure3: Top: CAD Model of the prototype imaging system, Above: Prototype Imaging system at the University of Glasgow

Identification of the two struck fibres per module (one in both x and y layers) yields one space point Fig. 4). With a single space point reconstructed per module (2 above and 2 below the imaged object - Fig. 1) the initial and scattered muon trajectories can then be determined for input into the imaging analysis software.

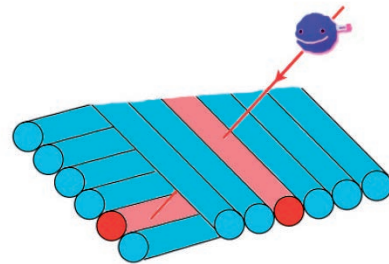


Figure 4: Perpendicular fibres (one in x- and one in y-direction) struck by an incident muon

Image Reconstruction

Images of the container contents are reconstructed using a statistical technique known as Maximum Likelihood Expectation Maximisation (MLEM) and to do this the project has developed an iterative algorithm developed from the work by Schultz *et al* [6]. Prior to performing the imaging analysis, the assay volume is divided into small volume elements called voxels. The dimensions of these voxels are pre-determined by the analyser and influenced by the necessary data collection duration and achievable image resolution in the x and y directions (i.e. smaller voxels provide greater definition in the final images but require a longer collection period due to fewer muons passing through their smaller volume).

In the analysis, the incoming and outgoing (Coulomb scattered) trajectories of every muon that passes through the acceptance of the detector (i.e. depositing signals in all eight detector layers) are back-projected to their Point of Closest Approach (PoCA). Provided that these two trajectories are within a pre-set tolerance (referred to as the Distance of Closest Approach or DoCA) of each other at this position, the MLEM algorithm determines a normalised probability of scattering in each voxel that the muon was considered to have passed through. This probability is weighted in each voxel by several factors including the path length of the muon within that element.

After many muons had passed through the system, the most likely scattering density λ (Eq. (1)) in each voxel is calculated via an iterative procedure that begins with an initial λ value pre-assigned in each voxel. This is conventionally set to the expected value of the predominant material within the system i.e. air or concrete for the prototype measurements. This ensures quicker convergence of the λ values, which are used as the imaging metric in all the results presented in the following section.

Using this method a density profile of the materials present within the imaging volume is produced (with high-Z materials have a larger λ value than lower-Z materials). This information is used to create the images, which are presented in the next section.

Results

'Bar' Images – Uranium and Lead in Air

Data collection commenced in late 2012 with a test configuration of objects placed within the imaging volume. This setup, shown in Fig. 5, which consists of a stainless-steel cylindrical bar measuring 12 mm in diameter positioned through a 40 mm cube of lead. A machined cylinder of uranium metal, 20 mm in diameter and 30 mm in length, is suspended beneath the bar. This steel bar is fixed to the aluminium profile support frame.

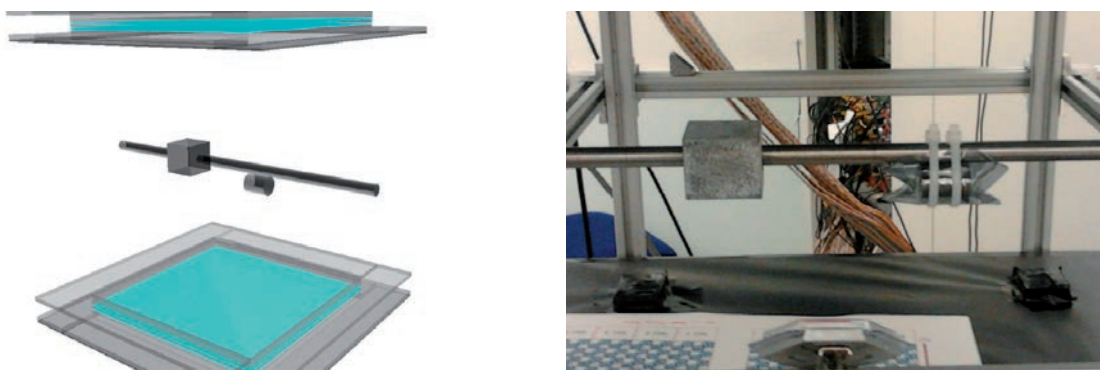


Figure 5: Left: Monte Carlo simulation of the lead and uranium samples attached to the steel bar. Right: Experimental arrangement (with the lead (left) attached and uranium (right) suspended below the steel bar (centre)).

Fig. 6 shows a comparison between the predicted results (from Monte Carlo simulation) and the experimentally obtained results from the small-scale prototype imaging system [7]. The images were obtained after several weeks of exposure to cosmic ray muons and show a sensitivity to atomic number Z and discrimination between the λ values of the stainless steel bar, the two high-Z material blocks, and the surrounding air. It can clearly be observed that there is very nice agreement between the predicted and measured images, with close agreement between them.

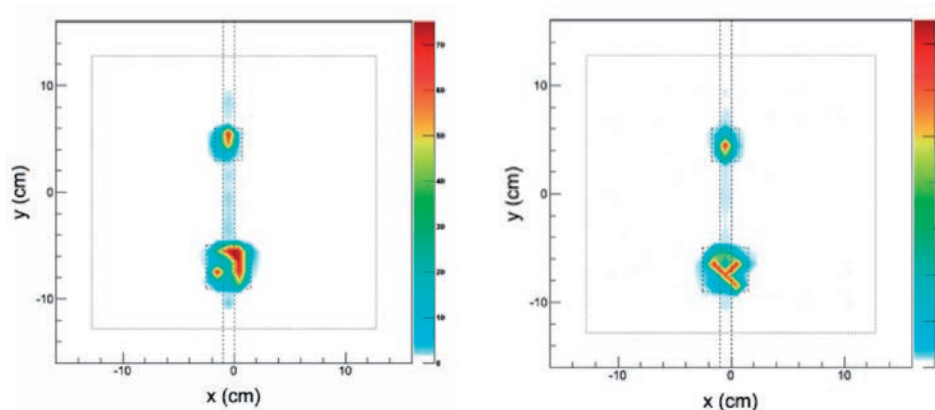


Figure 6: Left: Experimental results from the prototype imaging system showing the lead block (bottom) and uranium cylinder (top) – looking down on the steel bar. Right: Monte Carlo simulation results – with the same material geometry.

'Barrel' Images – Objects within a Miniature Concreted Barrel

After the success of the experimental arrangement described above a second experimental arrangement was implemented. This involved the imaging of materials (i.e. the uranium cylinder and lead block as described previously) that were placed within a cylinder (with several mm wall thickness) backfilled with dry concrete.

Fig. 7 shows the experimental arrangement of the barrel located within the imaging volume.

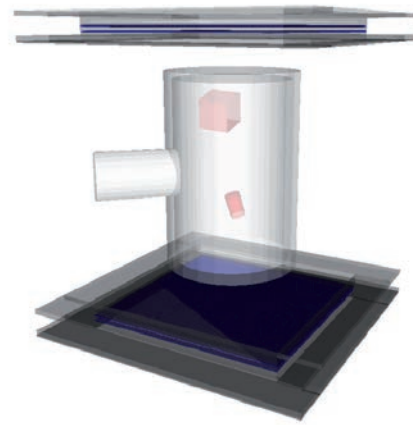


Figure 7: Left: Experimental arrangement of the concreted barrel placed within the imaging volume. Right: A simulated representation of the materials located within the barrel.

Fig. 8 shows the results of the experiment, with the location and dimensions of the uranium cylinder clearly visible in both the top-down (left) and side-on (right) images. This is a very impressive outcome and one that has helped in the development of the image reconstruction algorithms. The results clearly demonstrate the viability of deploying this technology to the imaging of high-Z materials located within concreted waste matrices.

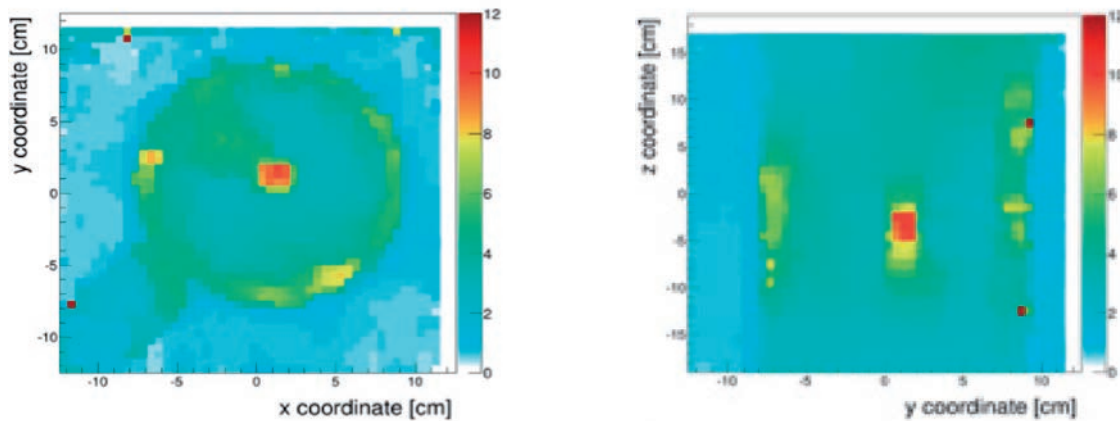


Figure 8: Left: Experimental data (looking down onto the top of the barrel) showing the uranium cylinder in the centre. Right: Experimental Data (looking from the side of the barrel) with the uranium cylinder shown at the centre.

Next Steps

Phase I of the project concluded successfully with the excellent imaging results which have been presented in this summary. The results of Phase I have been fed directly into Phase II of the project, which has the objective of developing a large-scale, prototype muon based imaging system, capable of imaging the density profile within 500 litre Intermediate Level Waste (ILW) containers. Phase II of the project is ongoing and will pave the way for moving the technology from a mid-TRL level to one that prepares the groundwork for final deployment of the technology at Sellafield Ltd. sites.

Acknowledgements

The author would like to gratefully acknowledge the funding from the Nuclear Decommissioning Authority and Sellafield Ltd. The work summarised in this article was undertaken by NNL and the University of Glasgow in collaboration as part of the ongoing Muon Tomography Project.

References

1. L. W. Alvarez, *Science*, **167**, 832, (1970).
2. K. Borozdin *et al Nature*, **422**, 277, (2003).
3. L. Schultz *et al.*, *Nuclear Instruments & Methods in Physics Research A*, **519**, 687, (2004).
4. C. Shearer, *Cosmic Muon Radiography – Feasibility Study Report*, NNL (10) 10895, March 2010.
5. A. Clarkson *et al.*, *Nuclear Instruments & Methods in Physics Research A*, **746**, 64, (2014).
6. L. Schultz *et al.*, *IEEE Transactions on Image Processing*, **16**, 1985, (2007).
7. D. F. Mahon *et al.*, *Nuclear Instruments & Methods in Physics Research A*, **732**, 408, (2013).

HYDROGEN YIELDS FROM WATER ON THE SURFACE OF PuO₂

Howard Sims

howard.sims@nnl.co.uk

Introduction

There is a large amount of plutonium dioxide (PuO₂) in storage around the world, including a large stockpile at the Sellafield site (Cumbria, United Kingdom). The vast majority of UK plutonium is derived from reprocessing of spent uranium metal fuels from UK Magnox reactors or oxide fuels from UK Advanced Gas Cooled reactors or foreign light water reactors and has accumulated over the last ~50 years. Current "Magnox" PuO₂ product is contained in an aluminium screw top container, inside a polyethylene bag and contained in a welded outer steel container. Similarly, plutonium derived from oxide fuels, reprocessed in the Thorp plant, is contained in a stainless steel screw top inner can held within a vented intermediate can placed inside a welded outer container. Conditions are carefully controlled during production and packaging to limit water adsorption into the plutonium powder and to meet acceptance criteria for storage. Very similar arrangements have been adopted by the United States Department of Energy for storing US plutonium (see DOE standard "3013").

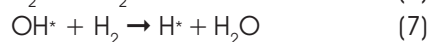
Of thousands of cans in stores only a few "out-of-specification" cans are known to have pressurised which empirically vindicates the acceptance criteria specified for storage. Even so, this is perhaps surprising because PuO₂ can adsorb many monolayers of water and it might be expected that this water would be radiolysed to hydrogen and oxygen; thus pressurisation should be observed even for cans that meet specifications for water content (measured *via* loss on heating [LOH] measurements). It is highly unlikely that at these high dose rates, typically 8 Wkg⁻¹, radiolysis does not occur so it must be assumed that a reverse reaction, such as recombination of radiolysis products on the surface of PuO₂, also occurs. So whilst there is plenty of operational experience in the safe and secure storage of plutonium in sealed canisters on nuclear licensed sites, there remains a clear need to underpin storage through better understanding of the fundamental chemical and physical processes that could lead to pressurisation; as well as radiolysis of water, there are other potential pressurisation mechanisms including helium generation from α -decay of plutonium isotopes, thermal desorption of water and, in Magnox cans, polythene degradation. Improved scientific understanding can also reduce some of the pessimisms built into stores' safety cases giving operational benefits such as allowing wider ranges of packages to be safely stored or package lifetimes to be extended.

In this article we summarize recently published experimental results on H₂ generation due to the radiolysis of water on PuO₂ surfaces; exploring the effect of dose rate, specific surface area (SSA) and number of water monolayers on the surface [1]. This work is part of a wider programme of studies at NNL that are supporting the safe storage of plutonium at Sellafield.

Background: radiolysis of water at a surface

Alpha radiolysis of water adsorbed on the surface of PuO₂ can result in the formation of hydrogen gas together with other molecular products. The actual mechanism of how this reaction occurs on the surface of PuO₂ remains under question. For instance, decomposition of adsorbed water following energy transfer to an interface may be quite different to radiolysis of that adsorbed water which in turn may occur by a quite different mechanism to radiolysis of bulk water. The energy deposition process in a few monolayers may be different from bulk water so that the concept of a "spur" and Linear Energy Transfer (LET) will not apply. Yields from alpha radiolysis in water are

different to gamma radiolysis, because of the higher LET of alpha radiolysis but this cannot apply in a few monolayers because the result of high LET is spur overlap but it is questionable whether even one spur will form in a few monolayers. However, it is almost certain that water is ionized by the passage of alpha particles so some of the initial processes for bulk water should apply Eq. (1-7):



It is also questionable whether products from second order reactions will form because reactions of radiolysis products (e_{aq}^- , $OH\cdot$) with the surface may dominate; this suggests reaction Eq. (7) is important. Much of this is speculation at present because the processes in monolayers are not known, for example, whether a hydrated electron e_{aq}^- will form in proximity to an oxide surface. Also if the oxide surface contains redox-active metal ions, reaction between the surface and radicals produced from water decomposition after energy transfer would not lead to excess hydrogen evolution. Understanding this surface chemistry provides a fundamental motivation for studies of water radiolysis at metal oxide surfaces.

Plutonium samples

In this work, production line samples of "Thorp" and "Magnox" PuO_2 were used to provide material with different specific activities and SSA. Also a "Magnox" PuO_2 sample that had been used for measurement of weight changes from heating (LOH analysis) was used. As this material had been heated to $>950\text{ }^\circ\text{C}$ the SSA was substantially reduced. These three samples thus provide variations in the number of monolayers of water that will be adsorbed onto the PuO_2 and the energy (dose) transferred to the adsorbed water molecules, the key factors that should determine radiolytic yields of H_2 . The SSA and specific activity (alpha) for each of the samples are given in Table 1. All of the samples were pre-dried in a dessicator before equilibration in gas tight tubes under air atmospheres of fixed relative humidities (RH) that varied from 0 to 95 %. All experimental work was carried out at room temperature. At the end of the equilibration period (samples reached a constant weight), gas samples were taken from the head space of each sample over a period of ~ 2 weeks. Samples of PuO_2 powder slurried in deionised water were also analysed; one of these was doped with sodium nitrite solution. H_2 was analysed using a micro-gas chromatograph and the rates of H_2 production then used to calculate a GH_2 value (*i.e.* molecules of H_2 formed per 100 eV of dose).

Table 1. SSA of PuO_2 samples

Sample	SSA (m^2g^{-1})	MeV(total) ($\text{s}^{-1}\text{g}^{-1}\text{Pu}$)
Magnox	8.9 - 1.1	2.9×10^{10}
Thorp	6.1 - 1.0	6.9×10^{10}
LOH	2.1 - 0.8	3.1×10^{10}
Slurry samples	8.9 - 1.1	2.8×10^{10}

Results

H_2 production rates were taken from the gradient of graphs of H_2 production vs. time; a typical example is given in Fig. 1; as expected these were linear over the period of analysis. Generally, better agreement was observed between the second and third datasets which may be due to some stabilisation of the experimental system. A noteworthy feature of the data is that in all cases the hydrogen production rate increased by an order of magnitude on increasing RH from 75 to 95 % whereas the number of monolayers (ML) of water (assuming 2 ML on the "dry" sample) increased by about a factor of ~ 3 .

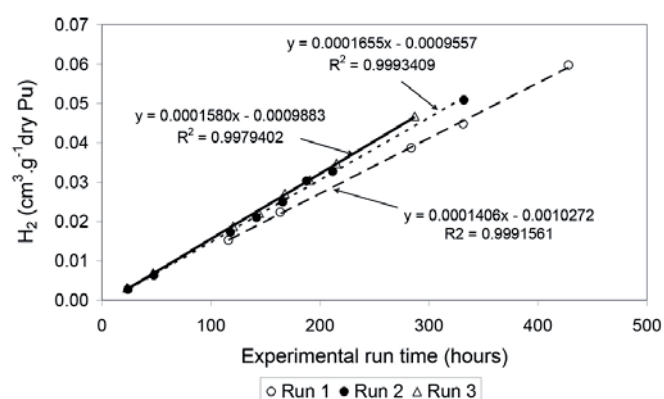


Figure 1: An example of H_2 yields (cm^3 per gram of dry PuO_2) vs. time for a typical sample (sample L95, *i.e.* LOH PuO_2 , 95 % RH). Data represents three separate runs under the same initial conditions

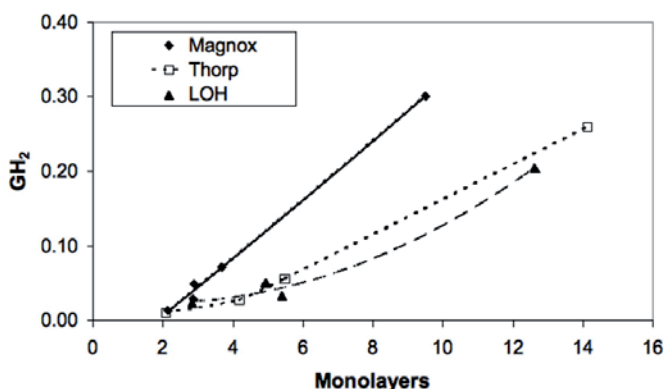


Figure 2: H_2 G-values (molec.100eV^{-1}) vs. number of calculated monolayers of water for Magnox, Thorp and low SSA ("LOH") PuO_2 samples (note: assumes 2 monolayers still present after room temperature drying in dessicators)

GH_2 vs. monolayer coverage of H_2O is plotted in Fig. 2. This shows significantly higher GH_2 for Magnox material which seems unlikely but it is a consequence of the lower number of monolayers of H_2O adsorbed on Magnox PuO_2 compared with Thorp and LOH material for a given RH. Alternatively, if GH_2 is plotted vs. RH much better agreement is observed as shown (Fig. 3). This may suggest that either SSA or water mass is not well known or alternatively not all of the BET-measured surface area is available for multi-monolayer adsorption of water (*e.g.* due to small pore sizes). The

important point, however, is that even at 95 % RH, GH_2 is about a factor of 4-5 below the accepted value for bulk water (*i.e.* 1.3 molec.100eV⁻¹). For comparison, the GH_2 values from the slurry experiments were 0.53 and 0.62 for the samples without and with nitrite doping respectively.

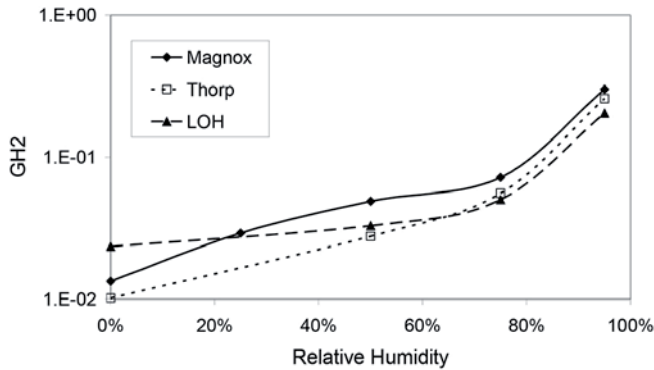


Figure 3: H_2 G-values (molec.100eV⁻¹) vs. Relative Humidity (%) for Magnox, Thorp and low SSA ("LOH") PuO_2 samples

The low values of GH_2 with low water coverage for PuO_2 are in contrast to data for UO_2 and CeO_2 , which are often considered as surrogates for PuO_2 . Here, the opposite trend was reported – *i.e.* very large GH_2 in the first few monolayers on CeO_2 and UO_2 surfaces. It is difficult to explain excess H_2 from UO_2 and CeO_2 but not PuO_2 . UO_2 might be expected to have a layer of U_3O_8 on the surface which would be expected to react with all radicals. CeO_2 cannot be oxidised but

can be reduced to Ce^{3+} so the excess H_2 might not be expected unless reduction of CeO_2 by H^\cdot and e^- is thermodynamically unlikely. CeO_2 can certainly be reduced by H_2 at around 470 K. An alternative explanation for the difference between CeO_2 and PuO_2 is that Ce_2O_3 and Pu_2O_3 are both thermodynamically unstable with water so although both CeO_2 and PuO_2 can be reduced, the sesquioxides will reduce water. However, in the case of PuO_2 the surface is known to contain Pu(V) so it may be this species that is reduced and the resulting Pu(IV) would not reduce water to H_2 . There is no equivalent Ce(V) species.

It is also of interest to compare results from this work with other results from the literature which are shown in Fig. 4. The data are rather scattered particularly below ~15 monolayers, probably reflecting the susceptibility of these data to factors such as variations in measured SSA, initial water content and experimental conditions. However, the figure clearly shows an increasing trend of GH_2 with the number of water monolayers or RH.

Regarding the slurry experiments, the ~17 % increase in GH_2 with nitrite present is consistent with a H_2 removal reaction by *e.g.* OH^\cdot radicals Eq. (8) followed by Eq. (9). The difference suggests that similar H_2 consumption reactions can occur on the surface of moist PuO_2 . The ratio of yields of the slurry to that expected from a homogeneous (aqueous) solution is $0.62/1.3 = 0.48$.

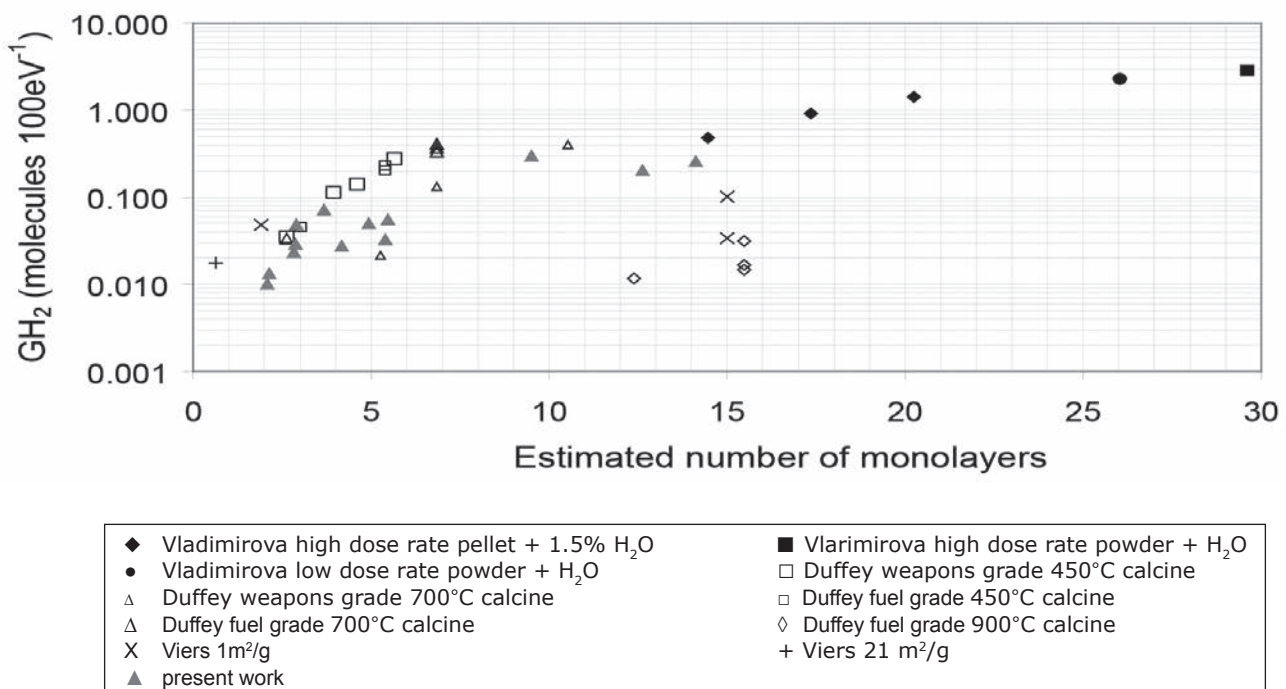
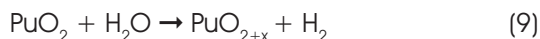


Figure 4: Comparison of available data for H_2 G-value (molec.100eV⁻¹) plotted against the number of calculated water monolayers on PuO_2 (present work = grey closed triangles; data of Viers and co-workers = cross symbols; data of Vladimirova and co-workers = closed symbols; data of Duffey and co-workers = open symbols. PuO_2 sources given in legend)

From our data the rate of production of H₂ from dry PuO₂ was about 10⁻⁵ cm³hour⁻¹gPuO₂⁻¹. Although this figure is subject to considerable uncertainty it can be shown that for a 7 kg can of PuO₂ this is equivalent to ~600 cm³ of H₂ per year assuming a gas volume in the can of 4 dm³; this is equivalent to 0.15 bar per year. As there is no sign of pressurisation normally in storage, then it must be concluded that there is an efficient removal mechanism such as recombination.

There has been debate in the literature [2] as to whether H₂ is formed via a radiolytic or thermal mechanism with the claim that there is a reaction Eq. (9):



It can be seen from data in this report that the rate of H₂ production is quite clearly dependent on water content and only becomes significant above ~4 monolayers. It is highly unlikely that a thermal reaction with water at the PuO₂ surface would be dependent on more than the chemisorbed and first physisorbed layers. Secondly, the H₂ production rate is dependent on dose rate which is not consistent with a thermal reaction. However, if the above discussion is correct and reactions of radicals with the surface can occur then production of H₂ could be accompanied by oxidation of the PuO₂ surface according to Eq. (10):



Conclusions

H₂ production rates from three different samples of Sellafield production line PuO₂ across a range of humid atmospheres have been measured. The results confirm the low production rates at low water monolayer coverage, increasing sharply between 75 and 95 % RH. These data show that the amount of hydrogen produced is dependent on the number of monolayers or RH and the specific activity of the PuO₂. These preliminary observations demonstrate that in our experiments H₂ production is a radiolytic rather than thermal process. Simple estimations based on hydrogen generation rates measured here indicate that there must be recombination reactions occurring within cans of PuO₂ that inhibit pressurisation under most storage conditions. An interesting observation is the higher H₂ production rate from Magnox PuO₂, which is of a lower specific activity than the Thorp plutonium; this may be related to the higher SSA and porosity.

Whilst our data fit trends from the literature the overall scatter in the data is unsatisfactory. However, it is clear that hydrogen production will be affected by a number of factors including the number of monolayers of water and the presence of other adsorbates (e.g. NO_x and CO₂). Further work is ongoing to reduce sources of uncertainty in these data and confirm the trends observed. Interestingly, some new, as yet unpublished

data, indicate an effect of atmosphere with radiolytic yields varying under air and N₂ atmospheres although overall our experience is showing that radiolytic generation of H₂ from H₂O adsorbed on PuO₂ is a complex phenomenon, influenced by many physical and chemical properties of the material. Future fundamental studies, in collaboration with the Universities of Manchester and Lancaster through the EPSRC funded "DISTINCTIVE" programme, will also focus on the factors that suppress H₂ generation close to the surface of the PuO₂.

Acknowledgements

We thank the UK Nuclear Decommissioning Authority and Sellafield Ltd. for support.

References

1. H.E. Sims, K.J. Webb, J. Brown, D. Morris, R.J. Taylor, *J. Nucl. Mater.*, **437**, 359, (2013).
2. J.M. Haschke, T.H. Allen, L.A. Morales, "Reaction of plutonium dioxide with water: formation and properties of PuO_{2+x}", *Science*, **287**, 285, (2000).

BEST AWARD

NNL is committed to developing technical and scientific experts within the lab. As part of the process it is imperative that we recognise talent within the business and provide an environment in which technical excellence can flourish. Excellent science is fundamental to the success of the NNL and should be celebrated.

Each year NNL awards the Lawrence Medal to the paper judged to be the Best External Scientific or Technical (BEST) publication. Any external publication with an NNL employee as a principal author is eligible for the award. This year there were 14 submissions for the BEST award. Each paper was assessed by a short listing committee and six papers made the shortlist on the basis of the technical and scientific content, the coherency of argument and the innovation and impact of the science.

The judging panel was chaired by Graham Fairhall, with Eann Patterson from Liverpool University as an external academic, and Senior Fellows Joe Small, Colin English and Kevin Hesketh. After considering the verdict it was decided that the BEST Award 2014 should go to Howard Sims for his paper 'Hydrogen Yields from water on the surface of plutonium dioxide'. Howard was given his award at the NNL Technical Conference in May and the paper is reported in this issue of NNL Science.



Howard Sims receiving his Lawrence Medal from Graham Fairhall



THE INAUGURAL NNL TECHNICAL CONFERENCE

The inaugural NNL Technical Conference took

place at the University of Manchester on 1st May 2014. This is the first in a series of annual conferences organised as part of the strategy to raise NNL's scientific and technical profile and showcase capability to both an external and internal audience.

The day was led and hosted by NNL's Chief Science & Technology Officer, Graham Fairhall, and featured an extensive programme of presentations from each of the NNL Businesses and Corporate R&D. These included:

Modelling PWR and BWR Fuel Crud Chemistry

- **Amit Agarwal**

Development of New Graphite Measurement Techniques in Support of Plant Lifetime Extension -

Nassia Tzelepi

The National Nuclear User Facility - **Simon Dumbill**
Americium-241 production for use in radioisotope power systems -

Mark Sarsfield

Robotics Autonomous Systems

- **Jim Harken and Bob Bowen**

Fuel Cycle Scenario Modelling - **Kevin Hesketh**

Hydrogen Yields from the surface of plutonium oxide

- **Howard Sims**

Alpha behaviour in SIXEP - **Zoe Maher**

Thermal Treatment of Wastes - **Charlie Scales**

Biogeochemistry and gas generation associated with the geological disposal of LLW/ILW -

Joe Small

NNL's Contribution to UK R&D Skills Strategy - **Katie Bell**

Nuclear Forensics - Every contact leaves a trace

- **Jeremy Edwards and Steve Baker**

Remote Deployment of Laser Techniques in

Decommissioning Environments - **Divyesh Trivedi**

There was also a keynote address from **John**

Perkins, Chief Scientific Advisor at the Department

for Business Innovation and Skills. A second guest

external presentation came from **Neil Smart**, R&D

Alliance Manager at Sellafield Ltd. Neil's presentation

examined 'Future Opportunities for Nuclear Research Supporting Sellafield'.



Over thirty external delegates attended the event from a range of NNL's customers and collaborators including: AMEC, Areva, AWE, BIS,

Cavendish Nuclear, DECC Science, EDF Energy, Environment Agency, Imperial College, Lancaster University, Leeds Metropolitan University, Leeds University, NDA, NIRO, Nuclear Institute, Rolls Royce, Sellafield Ltd, Sheffield University, The University of Manchester, Weinberg Foundation and Westinghouse.



“DISTINCTIVE” - Decommissioning, Immobilisation and Storage solutions for Nuclear waste Inventories

NNL's Central Lab hosted the afternoon session of the DISTINCTIVE Industrial Roadshow in July. DISTINCTIVE is a multi-million, four-year research programme that will combine the expertise of the nuclear industry with 10 universities to focus on some of the key challenges of the UK's nuclear legacy and to help build the next generation of nuclear experts.

NNL, NDA and Sellafield Limited are collaborating, along with the Engineering & Physical Sciences Research Council (EPSRC) and the consortium of UK universities on 30 separate projects which focus on four themes:

- AGR, Magnox and Exotic Spent Fuel
- Plutonium oxide and Fuel Residues
- Legacy Ponds and Silos Wastes
- Infrastructure characterisation, restoration and preservation

PHAROS (PHoton Analysis by Remote Observation Suite)



A recently established collaborative research group celebrated the launch of a new research laboratory on Friday 30 May

at The University of Manchester's Photon Science Institute. The PHAROS (PHoton Analysis by Remote Observation Suite) Laboratory forms the centrepiece of the collaboration between The University of Manchester's Laser Processing Research Centre (LPRC) and the National Nuclear Laboratory's (NNL's) Environmental Characterisation Team.

Research at the PHAROS Laboratory is currently focused on the development of at-a-distance, laser-based characterisation instrumentation techniques. The work is specifically aimed at remote, in-situ real-time materials identification, characterisation and monitoring in nuclear industry environments, such as during the decommissioning of nuclear plants. Initial research has involved the creation of a Laser-induced Breakdown Spectroscopy (LIBS) spectral characterisation library for nuclear materials, and the design, creation and successful testing of a remote Raman spectrometer utilising telescopic optics for the in-situ identification of materials over several metres.

The launch was attended by key staff from The University of Manchester and NNL and by VIP visitors from Sellafield Ltd. Speeches to introduce the new facility, explain the research work being undertaken and acknowledge those involved in this were given by NNL Chief Technologist Dr Mike

Angus and by Co-Director of The University of Manchester's Dalton Nuclear Institute, Professor Melissa Denecke. Demonstrations of some of the laboratory's equipment (which comprise a LIBSCAN 100 Laser-induced Breakdown Spectroscopy (LIBS) instrument, a prototype remote laser-based Raman spectrometer, a mobile 3D laser scanner, and a scanning electron microscope) were given during the event.

The PHAROS research group currently comprises Professor Lin Li (Head of LPRC), Dr David Whitehead (Senior Laboratory Manager), Dr Divyesh Trivedi (NNL Research Fellow), Dr David Hodgetts (Senior Lecturer within the University's School of Earth, Atmospheric and Environmental Sciences, and leader of research into the use of 3D Light Detection & Ranging (LiDAR), and MSc student Yibo Sun, who will be examining how to increase the range of remote Raman spectroscopy in nuclear industry environments. The group is currently led by Royal Society Industry Fellow and Visiting Professor Nick Smith, who is seconded to the University for 50% of his time from NNL where he is also NNL's lead geologist.



The PHAROS Laboratory gratefully acknowledges The University of Manchester's Photon Science Institute, Dalton Nuclear Institute,

and Schools of Mechanical, Aerospace and Civil Engineering (MACE), and Earth, Atmospheric and Environmental Sciences (SEAES) for infrastructure and personnel assistance. The team gratefully acknowledge NNL's Signature Research Programme, The University of Manchester, the University's Dean's Engineering and Physical Sciences Award Scheme, and the Royal Society for current funding.

AUTHORS' BIOGRAPHIES



Robin Taylor (C.Chem., FRSC) is the National Nuclear Laboratory's Senior Laboratory Fellow for Actinide Chemistry based at the NNL's Central Laboratory. He has over 20 years experience in advanced reprocessing research and flowsheet development. A recent highlight was leading NNL's contribution to the development of the EURO-GANEX process as part of the European Framework VII project "ACSEPT"; a collaborative effort between NNL and European national labs from France, Germany and the EU's Joint Research Centre.



Howard Sims is the National Nuclear Laboratory fellow in Radiation Chemistry based at Harwell. He has worked for UKAEA and successor organisations for 37 years working on radiochemical and radiation chemical topics which have come together in recent work on radiation chemistry on the surface of PuO_2 . He has worked closely with the University of Manchester and has been involved in setting up their Dalton Cumbria Facility for radiation studies near Sellafield in West Cumbria.



Mark Bankhead (CChem) is an NNL research fellow in computational modelling and theoretical chemistry. He has 12 years' experience within the nuclear industry. His main research interests are numerical simulation of chemical thermodynamics and kinetics at interfaces and transport properties in porous materials using *Ab Initio*, molecular and meso-scale simulation methods and chemical thermodynamics. Mark is also an expert on High Performance Computing and is the technical lead for NNL's HPC computational facility.



Colin Gregson is a Senior Research Technologist based at the NNL's Central Laboratory, Sellafield. He has been involved in R&D programmes from waste characterisation within legacy ponds (Corroded Magnox Sludge and soluble plutonium speciation), the development of advanced reprocessing flowsheets for spent fuel incorporating minor actinide partitioning and plutonium dioxide radiolysis and dechlorination studies. Colin also provides technical support to both Magnox and Thorp reprocessing.



Jonathan Austin is a Senior Research Technologist in the Plant and Process Optimisation team at NNL. Jonathan has a PhD in quantum mechanics (QM) modelling of heavy elements from the University of Manchester. In 2009 Jonathan joined the NNL, working in the Magnox effluents area, developing and applying process models of ion exchange and Magnox sludge chemistry. He also continues to work in the field of atomistic modelling, using QM to study the solids precipitated in highly active liquors and providing industrial supervision to three NDA funded computational chemistry PhD studentships at UCL.



Mike Carrott is a technical specialist in the Process Chemistry Team at the NNL's Central Laboratory. He has over 15 years supporting reprocessing operations for Thorp and Magnox plants and is also involved with development of advanced reprocessing flowsheets. Recently, this has included undertaking plutonium active trials for the development of the "EURO-GANEX" flowsheet for the European Framework Programme VII ACSEPT project.



Helen Steele obtained her BSc and PhD from the University of Manchester. Following a research fellowship at the Centre for Radiochemistry Research she joined NNL's predecessor in 2005. Her main interests are in actinide and surface chemistry. In 2012 she was awarded a CEA-Eurotalents fellowship to research actinide chemistry through quantum mechanical modelling, at CEA-Marcoule.

AUTHORS' BIOGRAPHIES



Scott Owens (PhD, CChem, FRSC) is the NNL Business Manager for the Plant and Process Optimisation Team and the Technical Lead in Chemical and Materials Modelling, with nearly 25 years experience in modelling throughout the nuclear fuel cycle. In addition to models of effluent treatment, Scott has made a significant contribution to understanding a range of fundamental modelling approaches, with applications in oxide fuel structure and morphology, molten salts processes, and glass and vitrification technology. Scott is the NNL Research Fellow to Imperial College London, where he lectures on undergraduate and postgraduate courses in Materials Science and Chemical Engineering.



Dominique Guillaumont is a research scientist at the CEA in Marcoule in the Radiochemistry and Processes Department in the field of computational actinide chemistry.



Philippe Moisy is a Research Director at CEA Marcoule. His interests include the study of actinide chemistry in aqueous solutions: solution chemistry and coordination chemistry (redox behavior of actinide and speciation) and recent research studies are focused on sonochemistry, electrochemistry and thermodynamics of concentrated solutions.



Manon Higgins-Bos (Ing, PhD, CChem) is a Technology Manager in the Plant & Process Optimisation Team at NNL. She has 20 years of experience in the area of effluent and ion exchange abatement technology. With a background in practical environmental and analytical chemistry, she completed a PhD in computational chemistry focussing on zeolite ion exchange. Manon is a committee member of the Royal Society of Chemistry's Statistical Mechanics and Thermodynamics Group and holds a post in the Sellafield Ltd. Effluents Technical Working Group.



Craig Shearer is the business manager for the Nuclear & Reactor Physics Team, within the Fuel and Radioisotopes business unit (FCS). Craig joined the NNL nuclear physics team in 2007 with a degree in Physics and a PhD in Nuclear Physics.

Craig has managed the Muon Tomography Project since 2009. Craig currently manages teams located across NNL (Sellafield, Springfield's and Risley) in addition to continuing to maintain overall management of the Muon Tomography Project which is based primarily at the University of Glasgow.



David Mahon is a research associate within the Nuclear Physics Group at the University of Glasgow. Since 2010, David has been employed as a software developer and data analyst within the Sellafield-funded Muon Tomography Project, overseeing the publication of the first imaging results earlier this year. David has a 1st Class degree in Physics and a PhD in Nuclear Physics. Throughout his time on the project, David has coordinated the image reconstruction software and simulation development, as well as leading collaborative studies into waste silo interrogation with INFN (Italy). In February 2013 in Vienna, David accepted the Elsevier Young Researcher of the Year on behalf of the project for his contribution.

- (1) D.W. Beardsmore; J.Q. da Fonseca; J. Romero; C.A. English; S.R. Ortner; J. Sharples; A.H. Sherry; M.A. Wilkes, Study of Luders phenomena in reactor pressure vessel steels, *Materials Science and Engineering A*, **588**, 151, (2013). *Structural Materials Properties Microstructure and Processing*, **2013**, 588, 151.
- (2) M.J. Carrot; C.R. Gregson; R.J. Taylor, "Neptunium Extraction and Stability in the GANEX Solvent: 0.2 M TODGA/0.5 M DMDOHEMA/Kerosene", *Solvent Extraction and Ion Exchange*, **31**, 463, (2013).
- (3) M. Dawson; D. Borman; R.B. Hammond; D. Lesnic; D. Rhodes, "A meshless method for solving a two-dimensional transient inverse geometric problem", *International Journal of Numerical Methods for Heat & Fluid Flow*, **23**, 790, (2013).
- (4) C.J. Donohoe; G.O.H. Whillock, "Localized Corrosion of Stainless Steel in a Nuclear Waste Cooling Water System-Part 7: Direct Radiation Experiments", *Corrosion*, **69**, 107, (2013).
- (5) H.R. Foxhall; K.P. Travis; L.W. Hobbs; S.C. Rich; S.L. Owens, "Understanding the radiation-induced amorphization of zirconolite using molecular dynamics and connectivity topology analysis", *Philosophical Magazine*, **93**, 328, (2013).
- (6) S. Gin; A. Abdelouas; L.J. Criscenti; W.L. Ebert; K. Ferrand; T. Geisler; M.T. Harrison; Y. Inagaki; S. Mitsui; K.T. Mueller; J.C. Marra; C.G. Pantano; E.M. Pierce; J.V. Ryan; J.M. Schofield; C.I. Steefel; J.D. Vienna, "An international initiative on long-term behavior of high-level nuclear waste glass", *Materials Today*, **16**, 243, (2013).
- (7) T.L. Griffiths; L.R. Martin; P.R. Zalupski; J. Rawcliffe; M.J. Sarsfield; N.D.M. Evans; C.A. Sharrad, "Understanding the Solution Behavior of Minor Actinides in the Presence of EDTA⁴⁻ Carbonate, and Hydroxide Ligands", *Inorganic Chemistry*, **52**, 3728, (2013).
- (8) S.F. Jackson; S.D. Monk; K. Lennox, "Testing of a scintillator and fibre optic based radiation sensor", *Radiation Measurements*, **59**, 50, (2013).
- (9) H. Kinoshita; P. Swift; C. Utton; B. Carro-Mateo; G. Marchand; N. Collier; N. Milestone, "Corrosion of aluminium metal in OPC- and CAC-based cement matrices", *Cement and Concrete Research*, **50**, 11, (2013).
- (10) F.W. Lewis; L.M. Harwood; M.J. Hudson; M.G.B. Drew; V. Hubscher-Bruder; V. Videva; F. Arnaud-Neu; K. Stamberg; S. Vyas, "BTBPs versus BTPHens: Some Reasons for Their Differences in Properties Concerning the Partitioning of Minor Actinides and the Advantages of BTPHens", *Inorganic Chemistry*, **52**, 4993, (2013).
- (11) E. Maddrell, "Hot isostatically pressed wasteforms for future nuclear fuel cycles", *Chemical Engineering Research & Design*, **91**, 735, (2013).
- (12) D.F. Mahon; A. Clarkson; D.J. Hamilton; M. Hoek; D.G. Ireland; J.R. Johnstone; R. Kaiser; T. Keri; S. Lumsden; B. McKinnon; M. Murray; S. Nutbeam-Tuffs; C. Shearer; C. Staines; G. Yang; C. Zimmerman, "A prototype scintillating-fibre tracker for the cosmic-ray muon tomography of legacy nuclear waste containers", *Nuclear Instruments & Methods in Physics Research Section a-Accelerators Spectrometers Detectors and Associated Equipment*, **732**, 408, (2013).
- (13) M.P. Metcalfe; A.W. Banford; H. Eccles; S. Norris, "EU Carbowaste project: Development of a toolbox for graphite waste management", *Journal of Nuclear Materials*, **436**, 158, (2013).
- (14) N. Paul; S. Biggs; M. Edmondson; T.N. Hunter; R.B. Hammond, "Characterising highly active nuclear waste simulants", *Chemical Engineering Research & Design*, **91**, 742, (2013).

- (15) S.L. Peck, "A human performance programme to improve front-line nuclear operations", *Cognition Technology & Work*, **15**, 29, (2013).
- (16) H.E. Sims; K.J. Webb; J. Brown; D. Morris; R.J. Taylor, "Hydrogen yields from water on the surface of plutonium dioxide", *Journal of Nuclear Materials*, **437**, 359, (2013).
- (17) D. Staicu; M. Barker, "Thermal conductivity of heterogeneous LWR MOX fuels", *Journal of Nuclear Materials*, **442**, 46, (2013).
- (18) S.J. Stanley; K. Lennox; A. Jenkins, "The development and testing of a much-improved Radball: A small deployable 360-deg-view radiation hot-spot imaging device", *Nuclear Technology* **2013**, 183, 260.
- (19) H.M. Steele; D. Guillaumont; P. Moisy, "Density Functional Theory Calculations of the Redox Potentials of Actinide(VI)/Actinide(V) Couple in Water", *Journal of Physical Chemistry A*, **117**, 4500, (2013).
- (20) P.D. Styman; J.M. Hyde; K. Wilford; G.D.W. Smith, "Quantitative methods for the APT analysis of thermally aged RPV steels", *Ultramicroscopy*, **132**, 258, (2013).
- (21) P. Swift; H. Kinoshita; N.C. Collier; C.A. Utton, "Phosphate modified calcium aluminate cement for radioactive waste encapsulation", *Advances in Applied Ceramics*, **112**, 1, (2013).
- (22) R.J. Taylor; C.R. Gregson; M.J. Carrott; C. Mason; M.J. Sarsfield, "Progress towards the Full Recovery of Neptunium in an Advanced PUREX Process", *Solvent Extraction and Ion Exchange*, **31**, 442, (2013).
- (23) P. Van Uffelen; P. Botazzoli; L. Luzzi; S. Bremier; A. Schubert; P. Raison; R. Eloidri; M.A. Barker, "An experimental study of grain growth in mixed oxide samples with various microstructures and plutonium concentrations", *Journal of Nuclear Materials*, **434**, 287, (2013).
- (24) S.H. Wallace; S. Shaw; K. Morris; J.S. Small; I.T. Burke, "Alteration of Sediments by Hyperalkaline K-Rich Cement Leachate: Implications for Strontium Adsorption and Incorporation", *Environmental Science & Technology*, **47**, 3694, (2013).
- (25) G.O.H. Whillock; C.J. Donohoe, "Localized Corrosion of Stainless Steel in a Nuclear Waste Cooling Water System-Part 6: Testing for Stress Corrosion Cracking Susceptibility", *Corrosion*, **69**, (2013).



Winner
RESEARCH & DEVELOPMENT
Sector Award

Winner 2004 - 2008, 2010 - 2011, 2014
Highly Commended 2009, 2012, 2013



5th Floor
Chadwick House
Warrington Road
Birchwood Park
Warrington
WA3 6AE

T. +44 (0) 1925 289800
E. customers@nnl.co.uk

W. www.nnl.co.uk

 @UKNNL

NATIONAL NUCLEAR
LABORATORY 